

Figure 1A A simplified PSK transmitter.

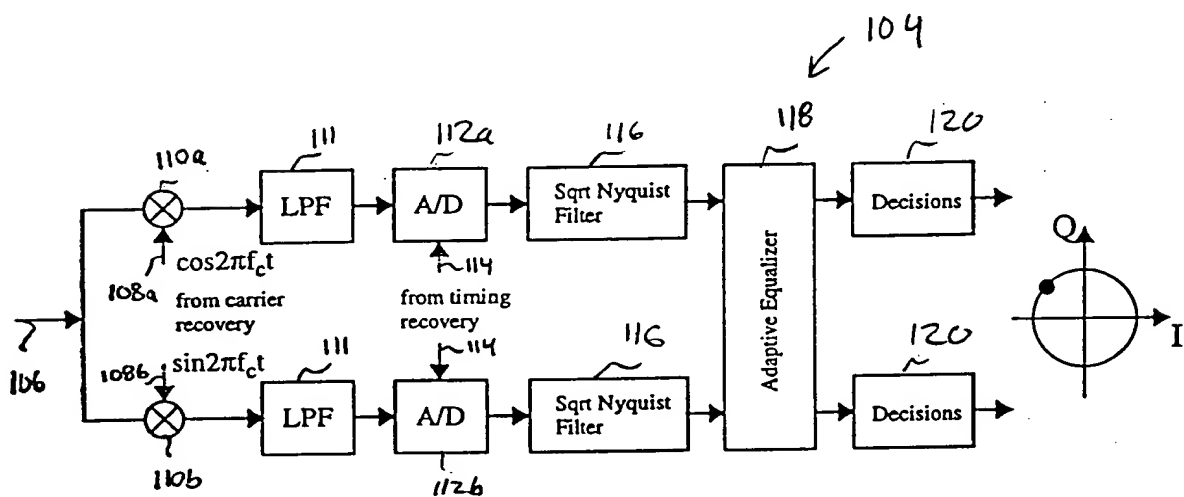
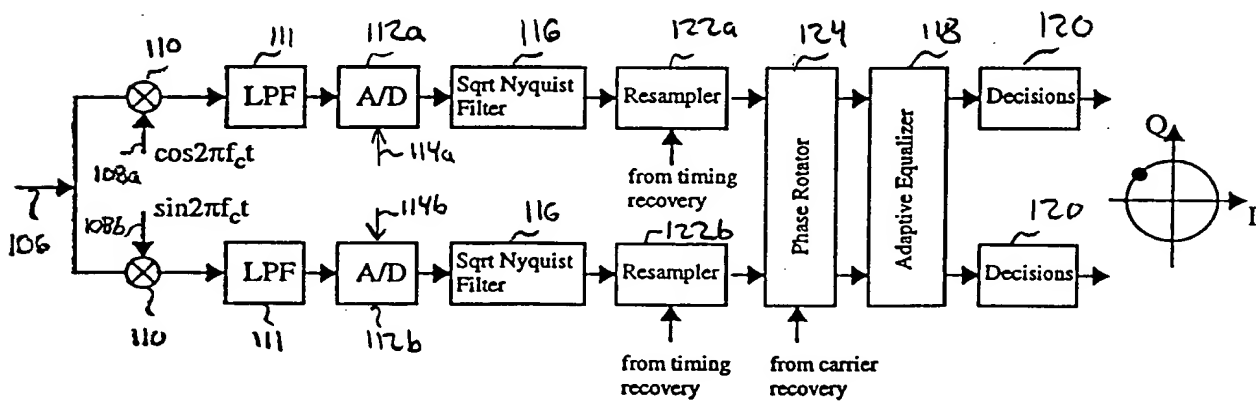
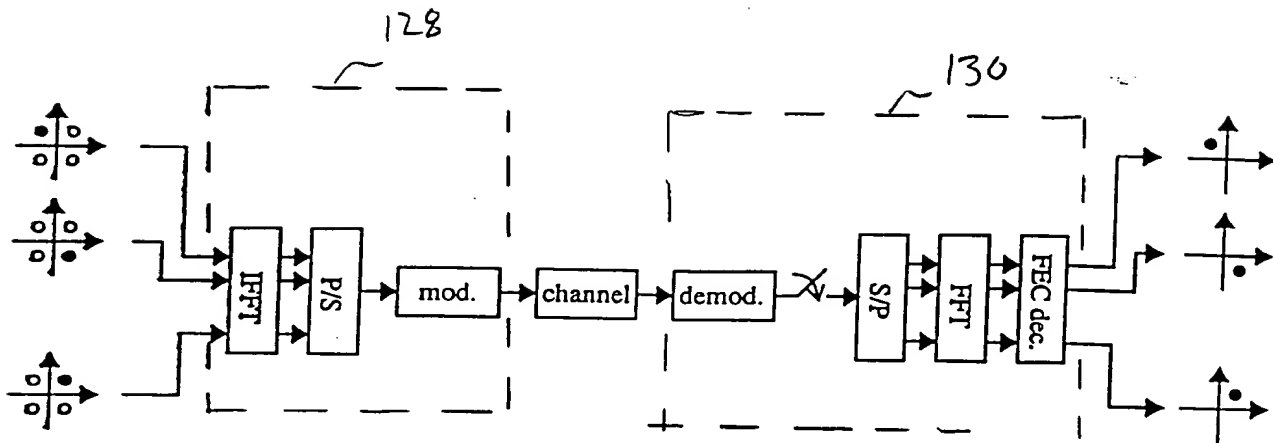


Figure 1B A simplified PSK receiver.



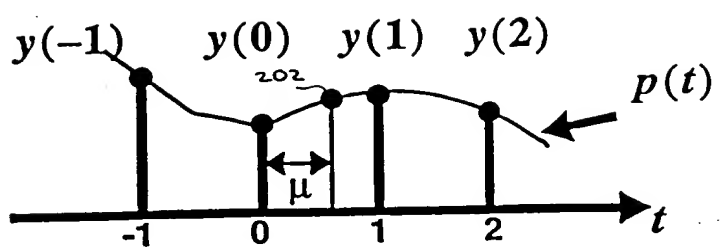
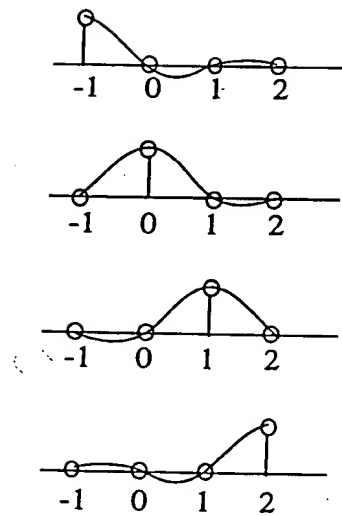


Figure 2 Interpolation Environment



$$C_{-1}(\mu) = -\frac{1}{6}\mu^3 + \frac{1}{2}\mu^2 - \frac{1}{3}\mu$$

$$C_0(\mu) = \frac{1}{2}\mu^3 - \mu^2 - \frac{1}{2}\mu + 1$$

$$C_1(\mu) = -\frac{1}{2}\mu^3 + \frac{1}{2}\mu^2 + \mu$$

$$C_2(\mu) = \frac{1}{6}\mu^3 - \frac{1}{6}\mu$$

Figure 3 The Lagrange basis polynomials.

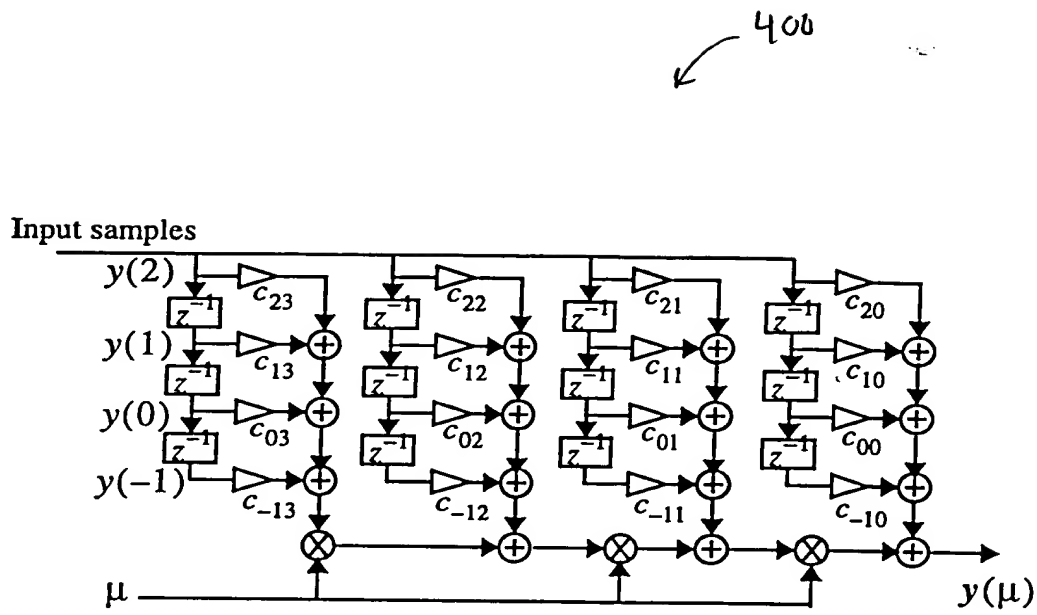


Figure 4 The Farrow structure that implements (2.5) and (2.6).

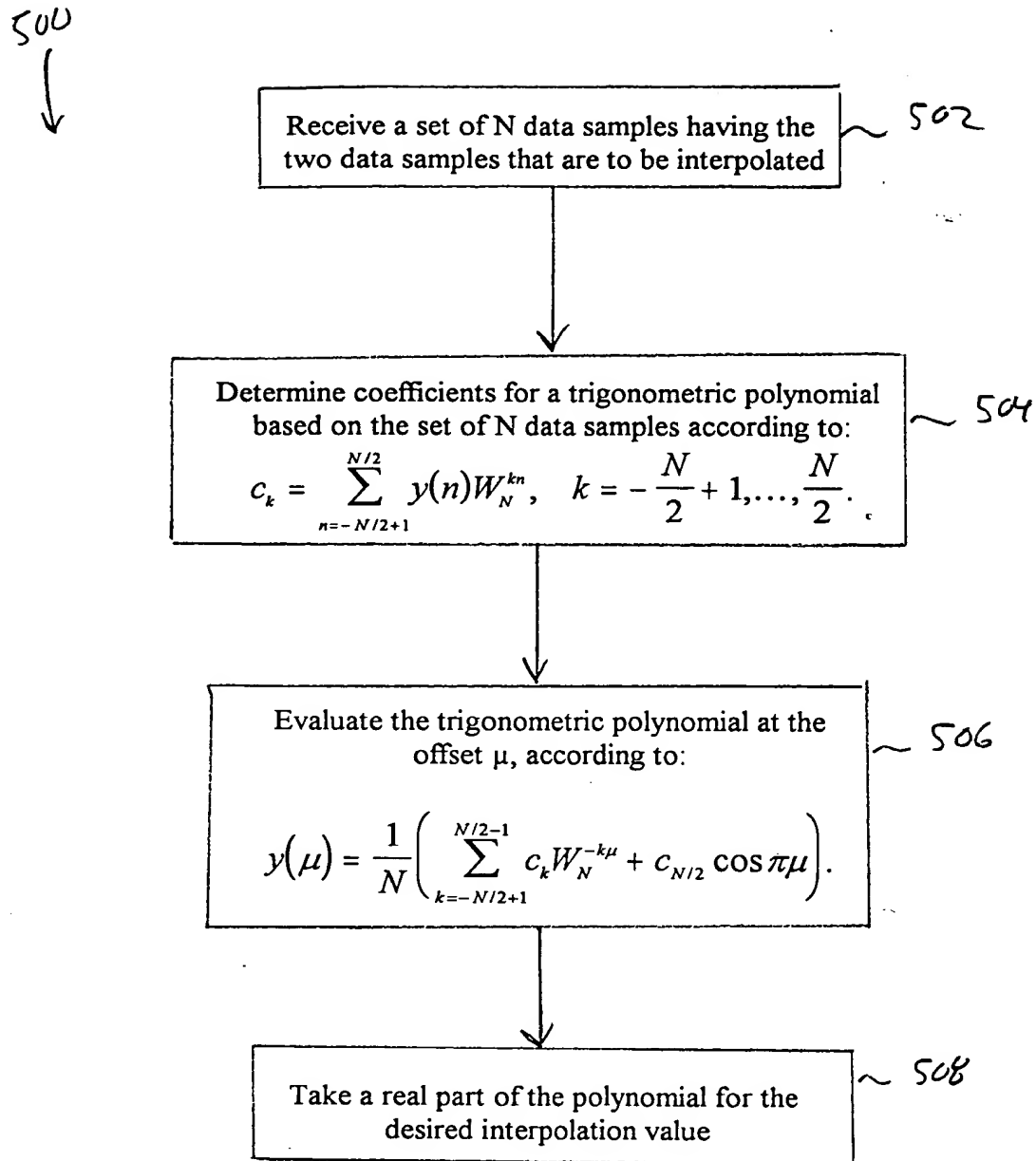


FIG. 5

FIG. 6A

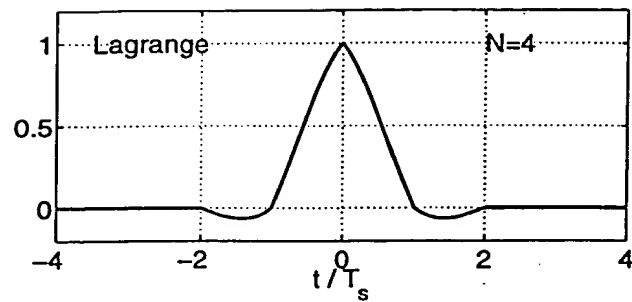


FIG. 6B

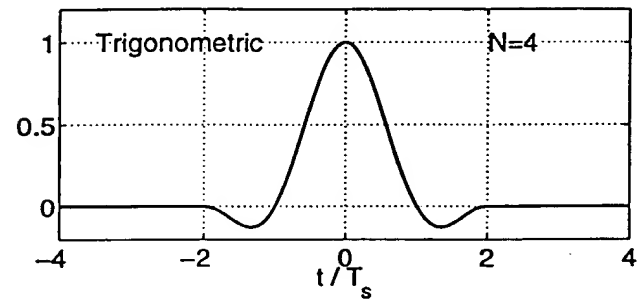


FIG. 6A-6B Impulse responses of (a) Lagrange interpolator and (b) Trigonometric interpolator.

FIG. 7A

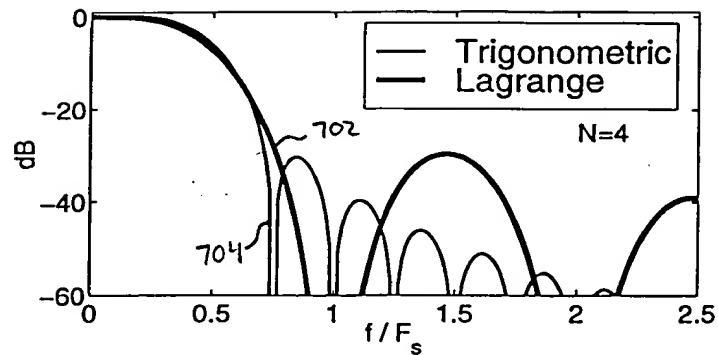


FIG. 7B

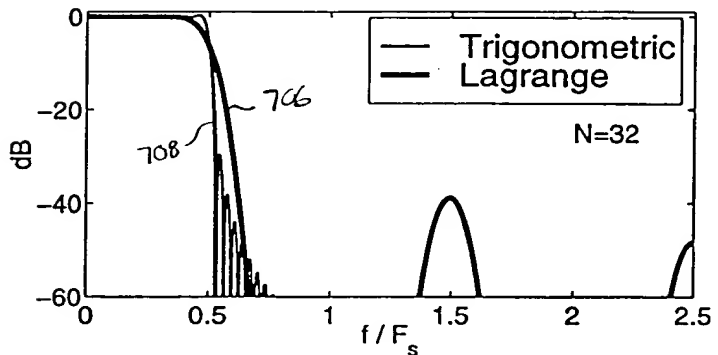


FIG. 7A-7B: Frequency responses for (a) $N=4$ and (b) $N=32$.

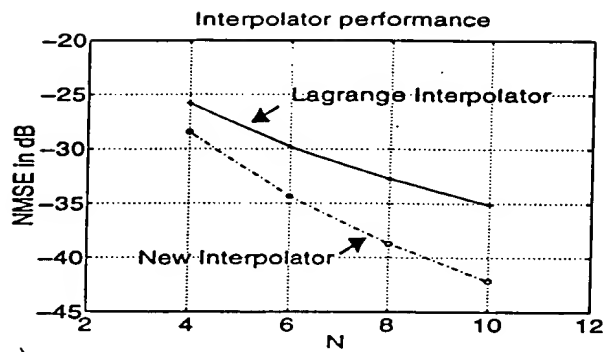


Figure 8B NMSE of the interpolated signal.

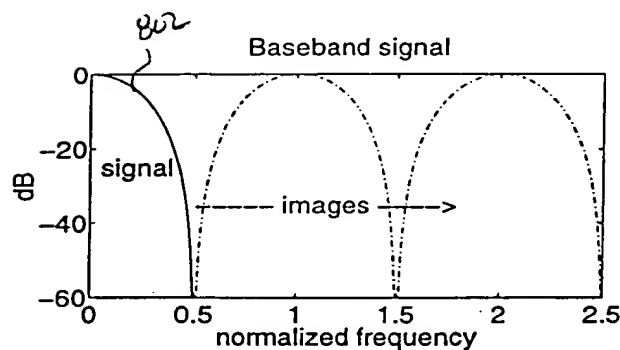


Figure 8A Signal with two samples/symbol and 100% excess BW.

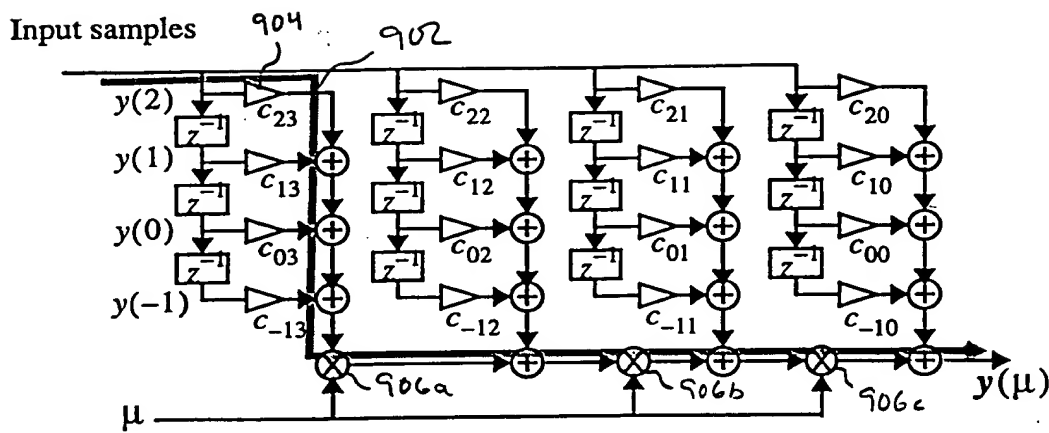


Figure 9 The critical path of the Lagrange cubic interpolator.

09698246 102000

lock

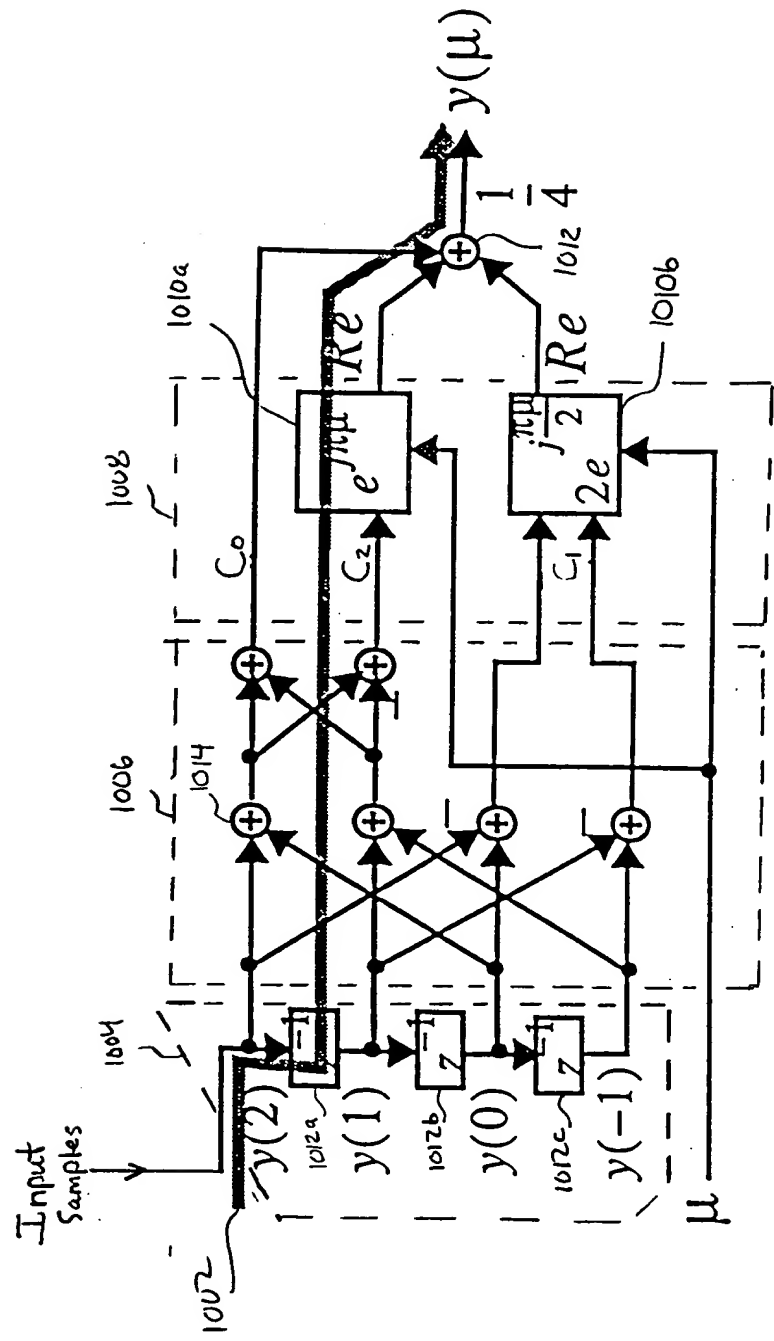


FIG. 10: Trigonometric Interpolator ($N=4$)

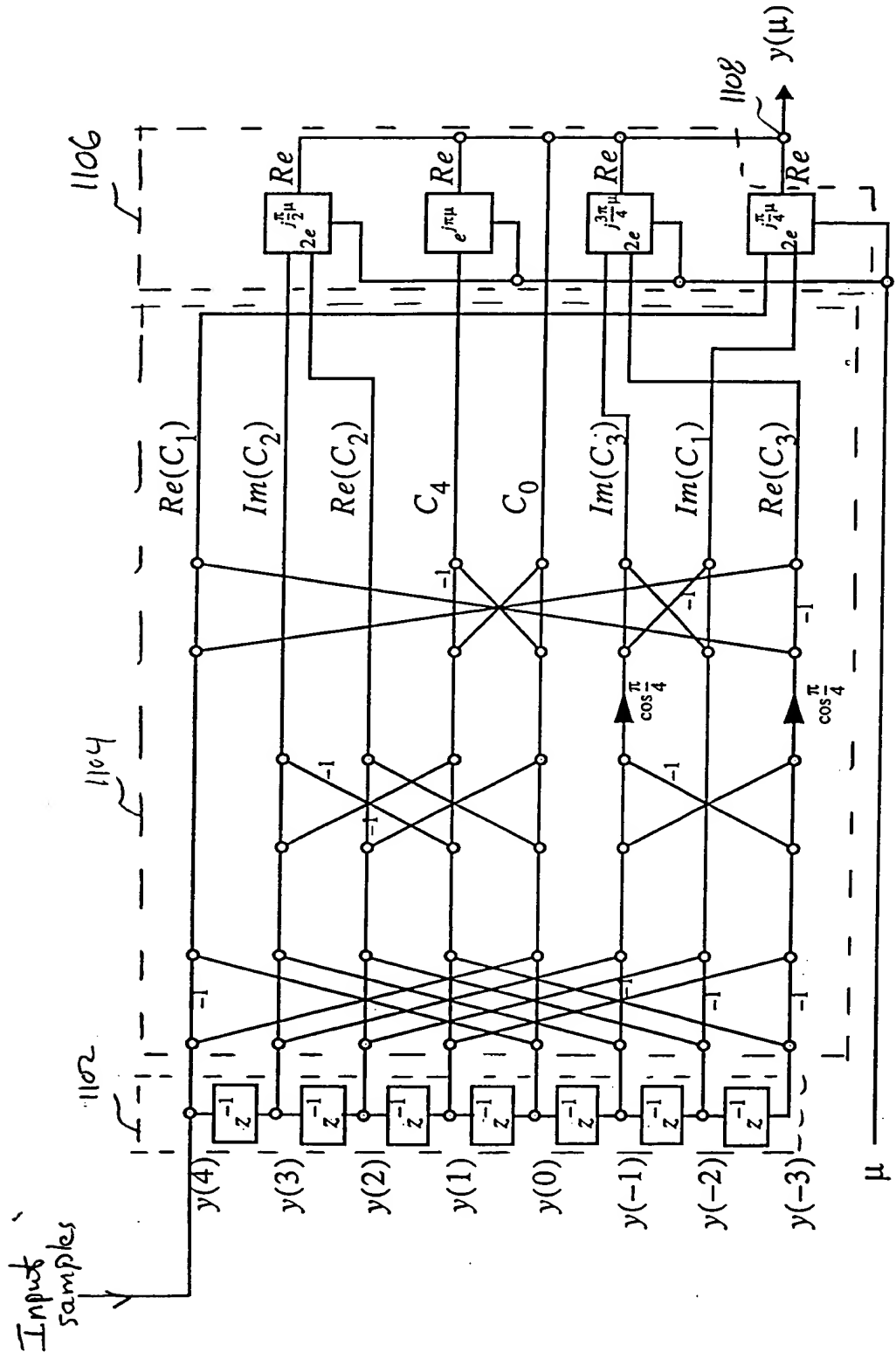


Figure 11 Trigonometric Interpolator with $N=8$.

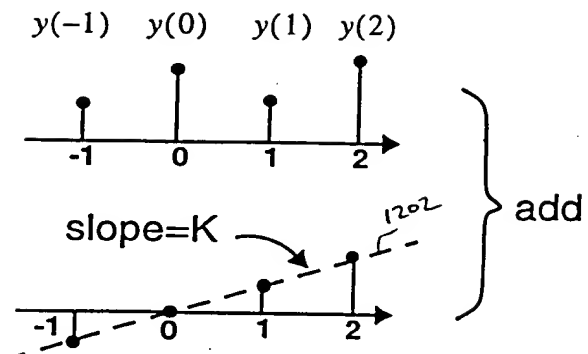


Figure 12 Conceptual modification of input samples.

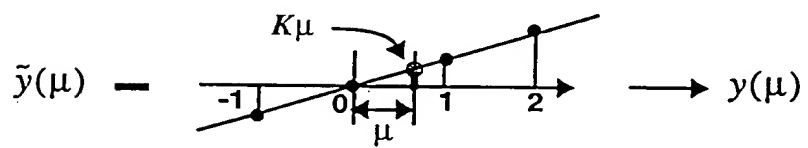


Figure 13 Correcting the offset due to modification of original samples.

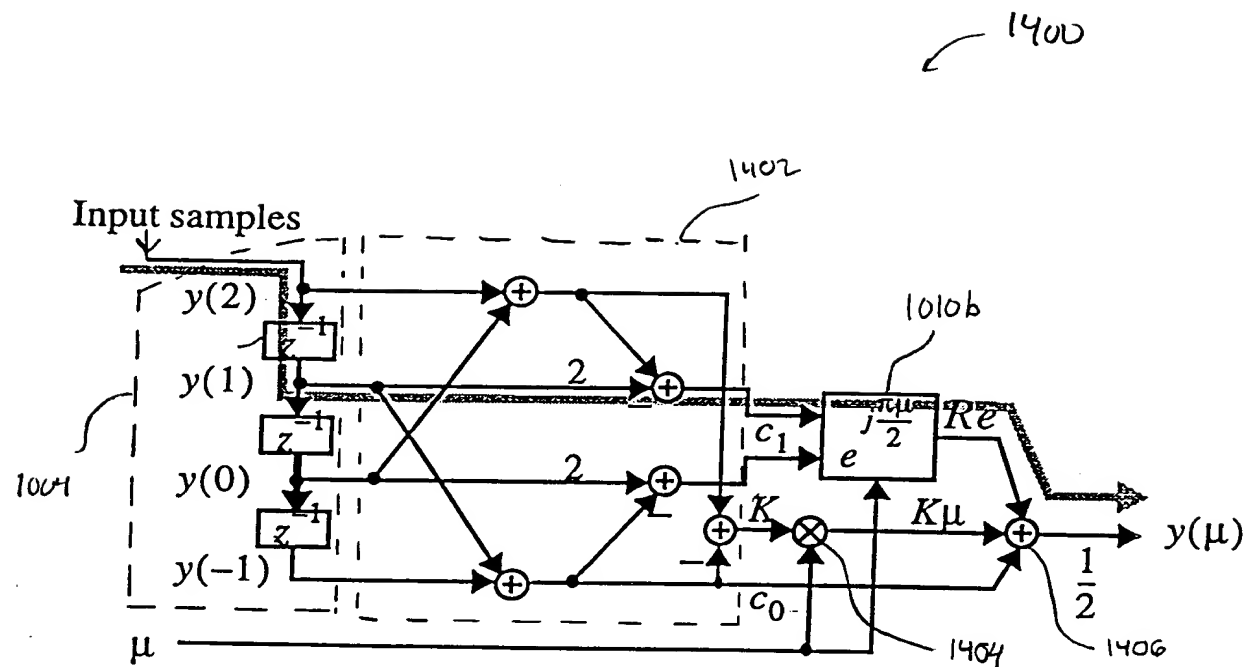


FIG. 14: Trigonometric Interpolator $N=4$

1500
↓

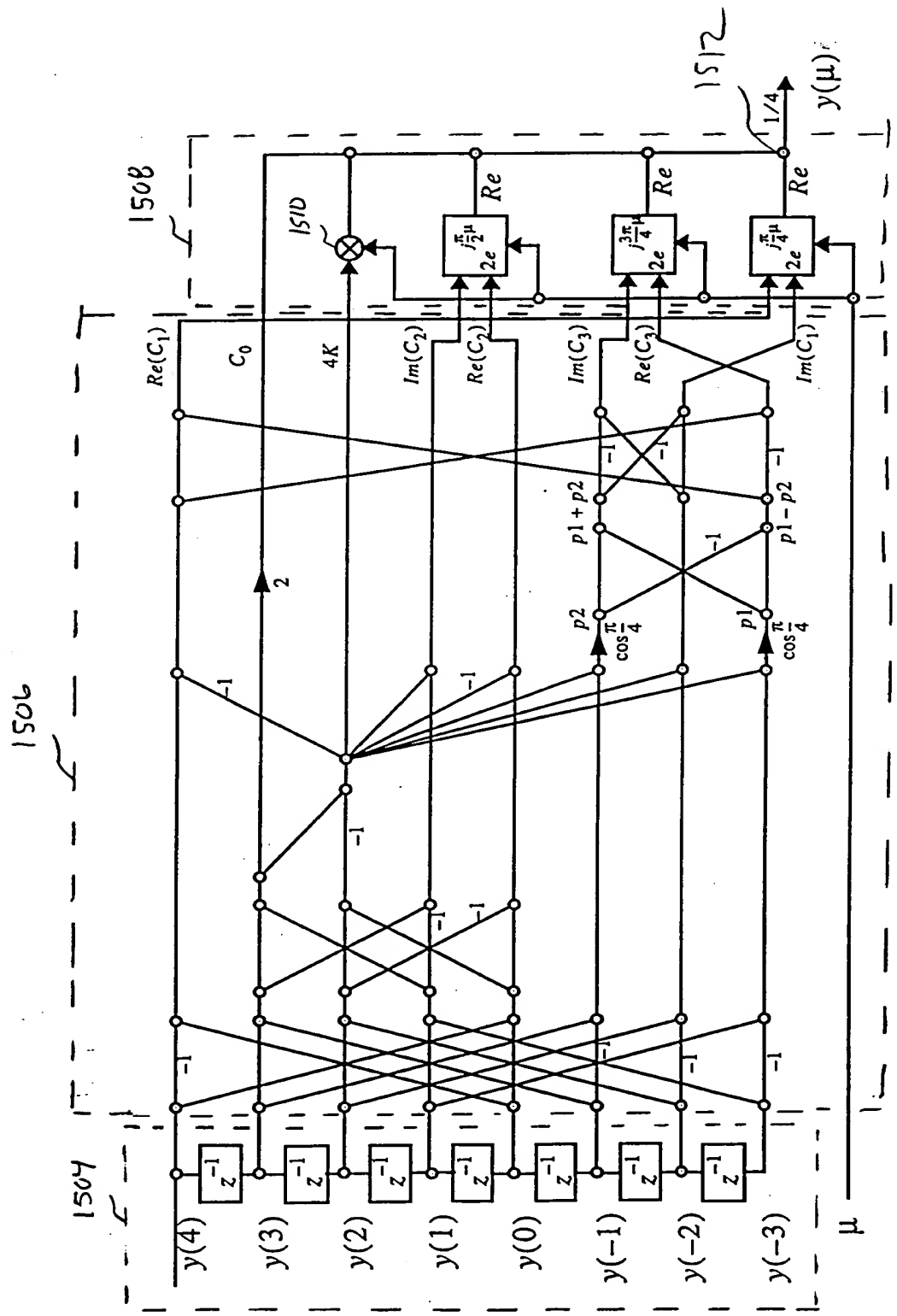


FIG. 15 The modified Trisonometric Interpolator

Interpolation errors are shown in gray.

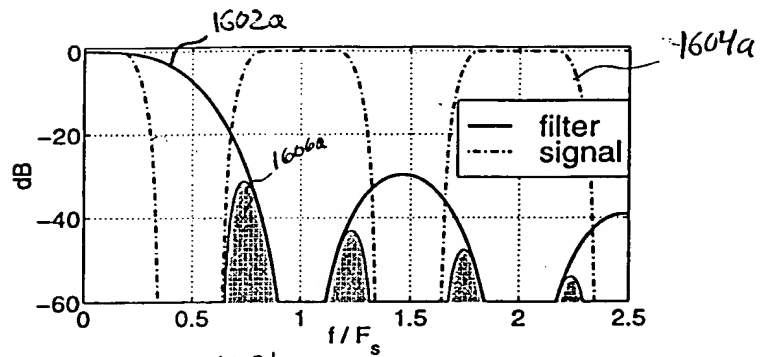


FIG. 16A: Lagrange cubic

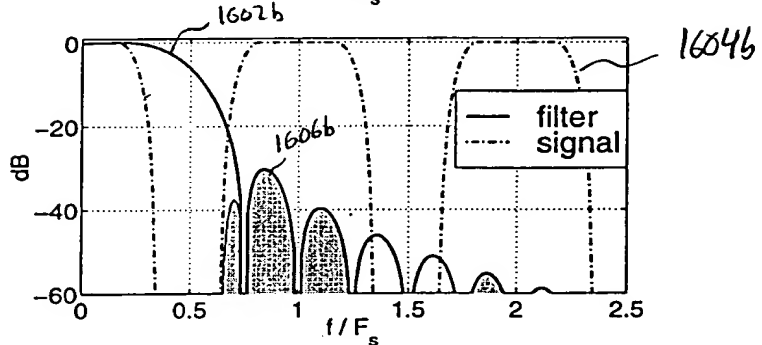


FIG. 16B: Trigonometric Interpolator 1000 (FIG. 10)

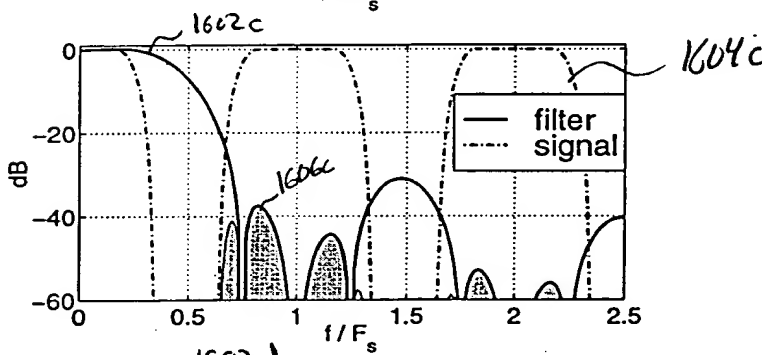


FIG. 16C: Trigonometric Interpolator 1400 (FIG. 14)

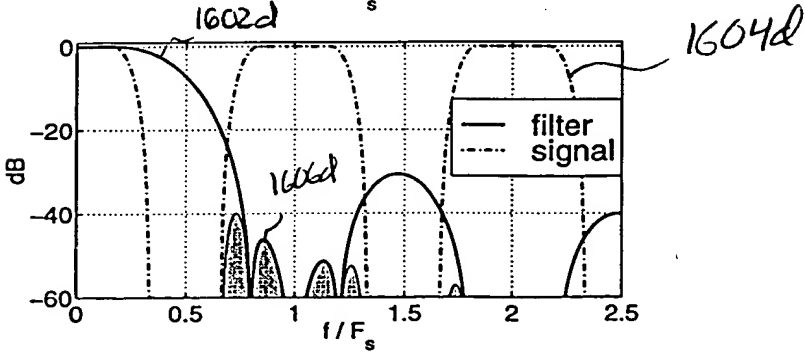


FIG. 16D: Optimal structure

1700



Receive a set of N input data samples

~1702

Delay the input samples

~1704

Generate one or more trigonometric coefficients
having one or more complex coefficients,
based on the delayed data samples

~1706

Rotate one or more of the complex coefficients in a complex plane
according to the offset μ

~1708

Add together the real parts of the complex coefficients, and
scale as necessary, resulting in the desired interpolation value
at the offset μ

~1710

FIG. 17

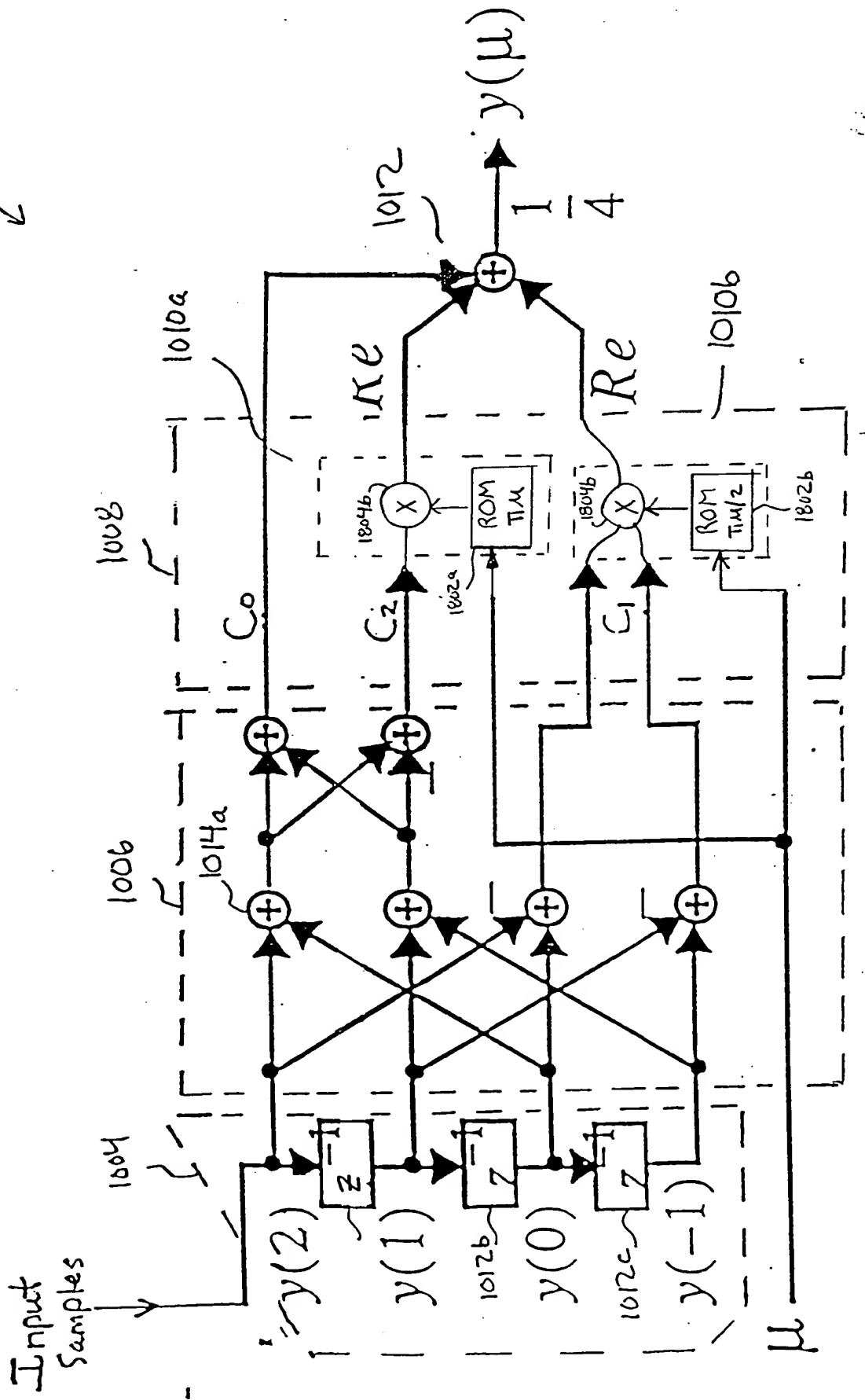


Fig 18

1900

Receive a set of N input data samples

1902

Delay the input samples

1904

Modify one or more of the data samples so that a coefficient $C_{N/2}$ is 0, according the following:

$$y(n)_{\text{mod}} = y(n) + n \cdot K;$$

$$K = -\frac{2}{N} \sum_{n=-N/2+1}^{N/2} (-1)^n y(n);$$

1906

Generate one or more trigonometric coefficients having one or more complex coefficients, based on the delayed data samples, wherein $C_{N/2}$ is 0

1908

Rotate one or more of the complex coefficients in a complex plane according to the offset μ

1910

Multiply the K factor by the offset μ to produce a $K\mu$ factor

1912

Add together the real parts of the coefficients and the $K\mu$ factor, resulting in the desired interpolation value.

1914

FIG. 19

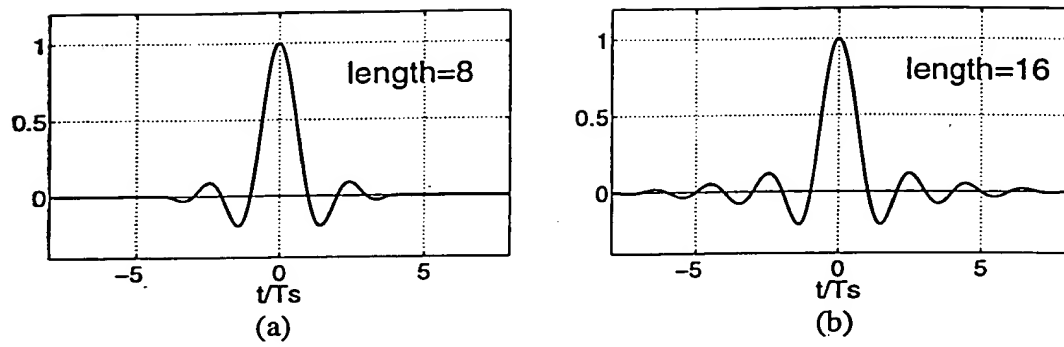


FIG.20: Normalized Impulse responses f of the interpolation filters.

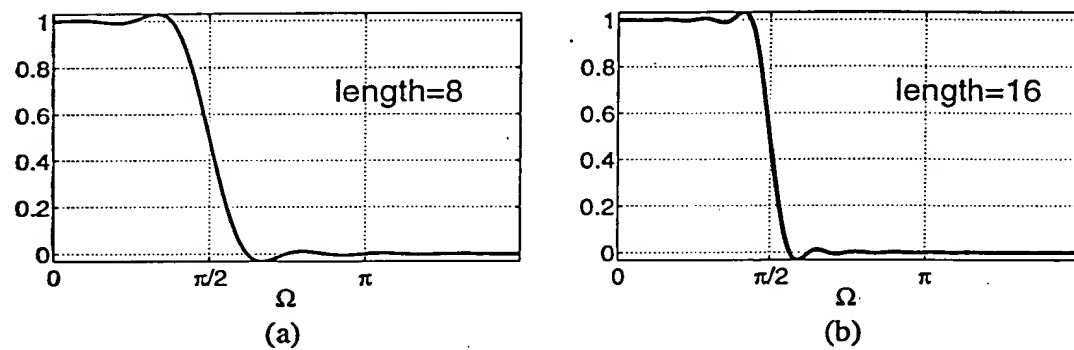


FIG.21: Normalized Frequency responses F of the interpolation filters.

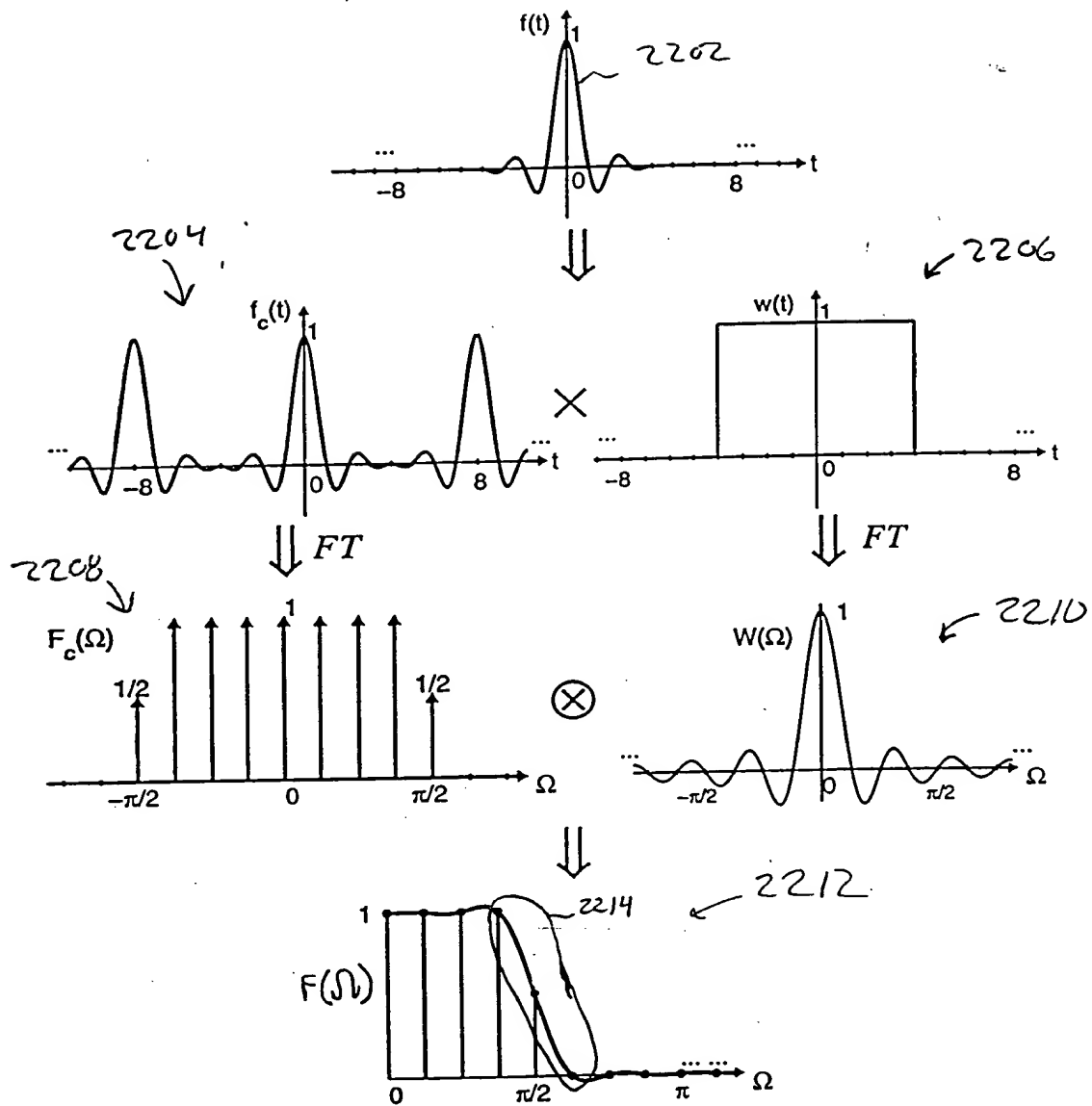


FIG.22: Analysis of the frequency responses.

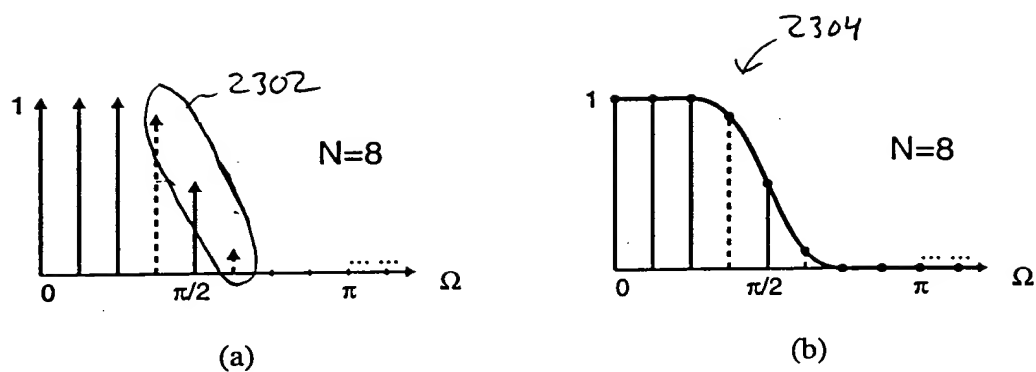


FIG.23 Effect of a more gradual transition at the band edge.

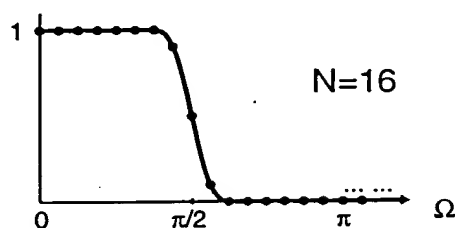


FIG.24 Reducing the transition bandwidth by increasing N .

3-4b, in which $N = 8$.

FIG.25A

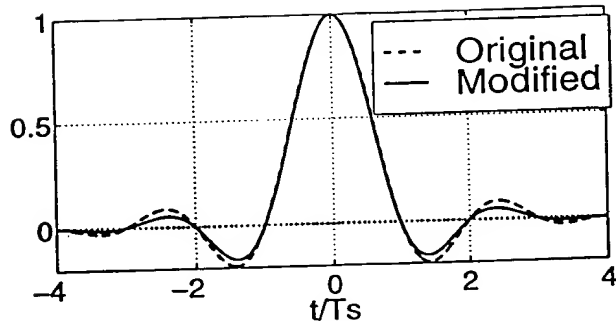


FIG.25B

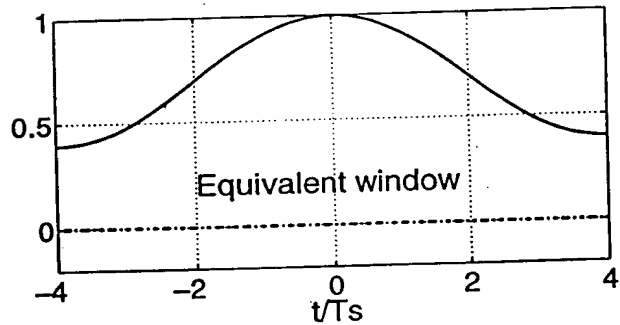


FIG.25A-B: (A) Impulse response of the original filter and the modified filter; (B) The equivalent window.

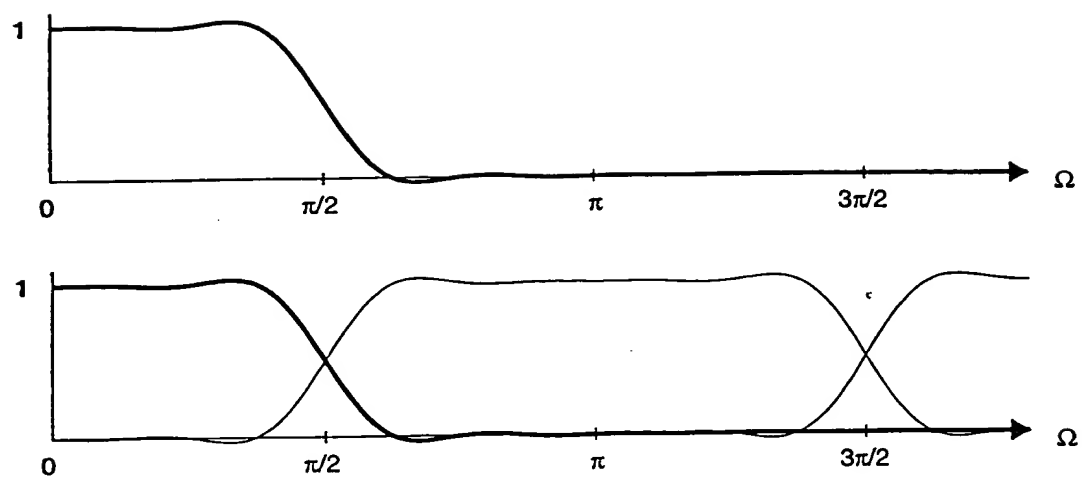


Fig. 26 Forming the frequency response of the discrete-time fractional-delay filter.

FIG. 27A

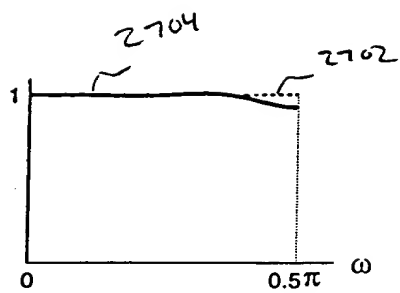


FIG. 27B

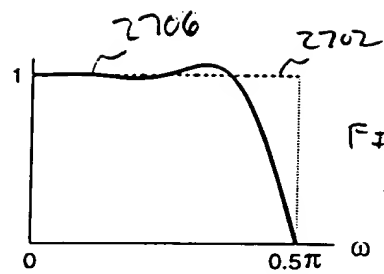


FIG. 27A-B : Fractional-delay filter with (A) $\mu=0.12$ and (B) $\mu=0.5$, using the preliminary $N=8$ interpolator.

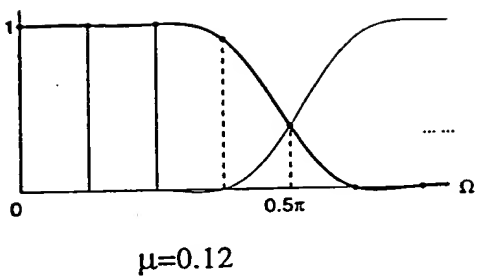
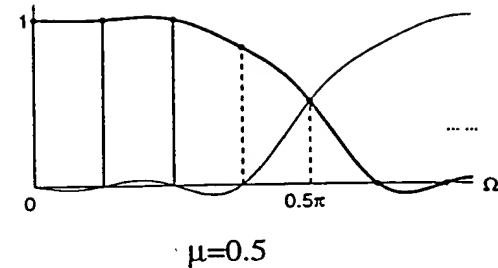
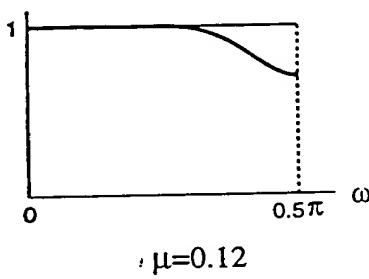
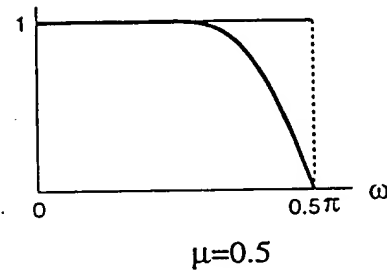
FIG. 28A $\mu=0.12$  $\mu=0.5$ FIG. 28C $\mu=0.12$ FIG. 28B $\mu=0.5$ FIG. 28D

FIG. 29A

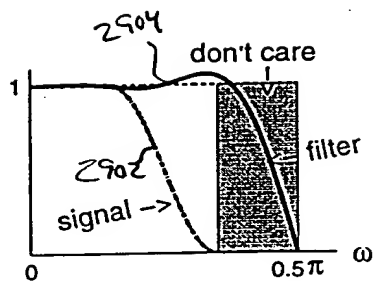
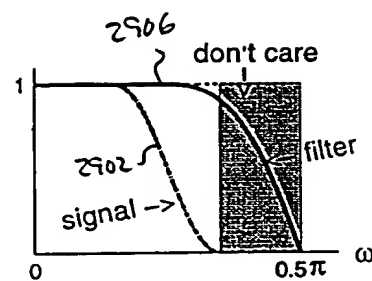


FIG. 29B

FIG. 29A-B : $F_\mu(\omega)$, with $\mu=0.5$, $N=8$, (A) before and (B) after optimization.

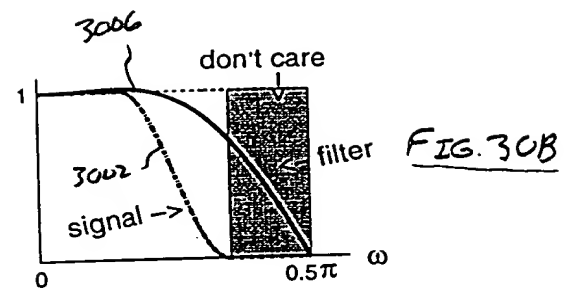
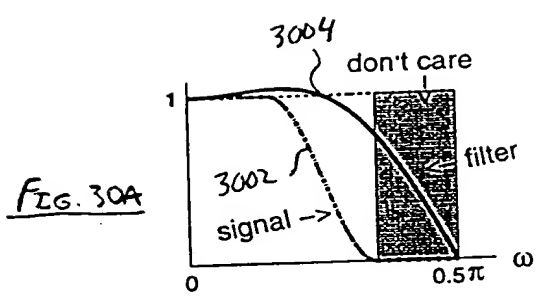


FIG. 30A-B $F_\mu(\omega)$ for $\mu=0.5$, $N=4$, A) before and B) after modification.

00000000000000000000000000000000

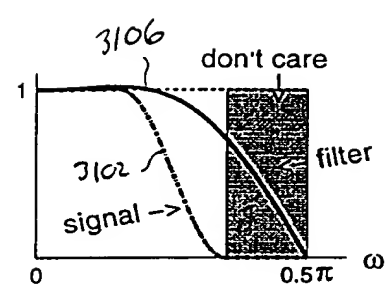
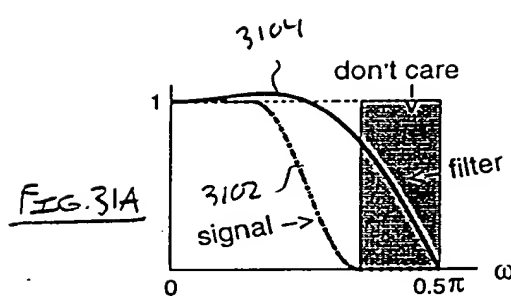


FIG. 31A-B $F_\mu(\omega)$, $\mu=0.5$, simplified $N=4$ structure, A: before and B: after modification.

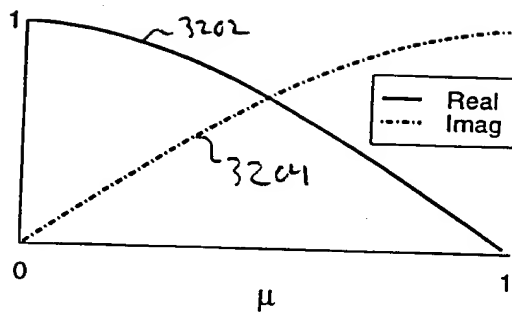


FIG.32: Real and imaginary components of the $F_{\mu(1)} e^{i \frac{\pi}{2} \mu}$ value.

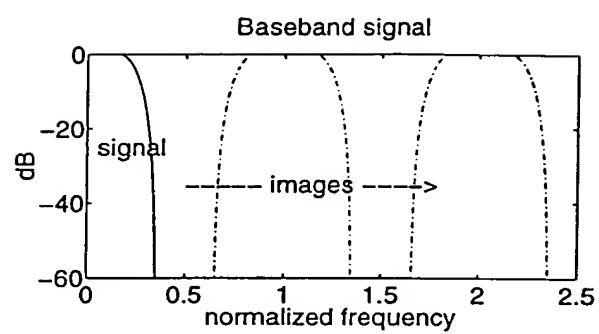
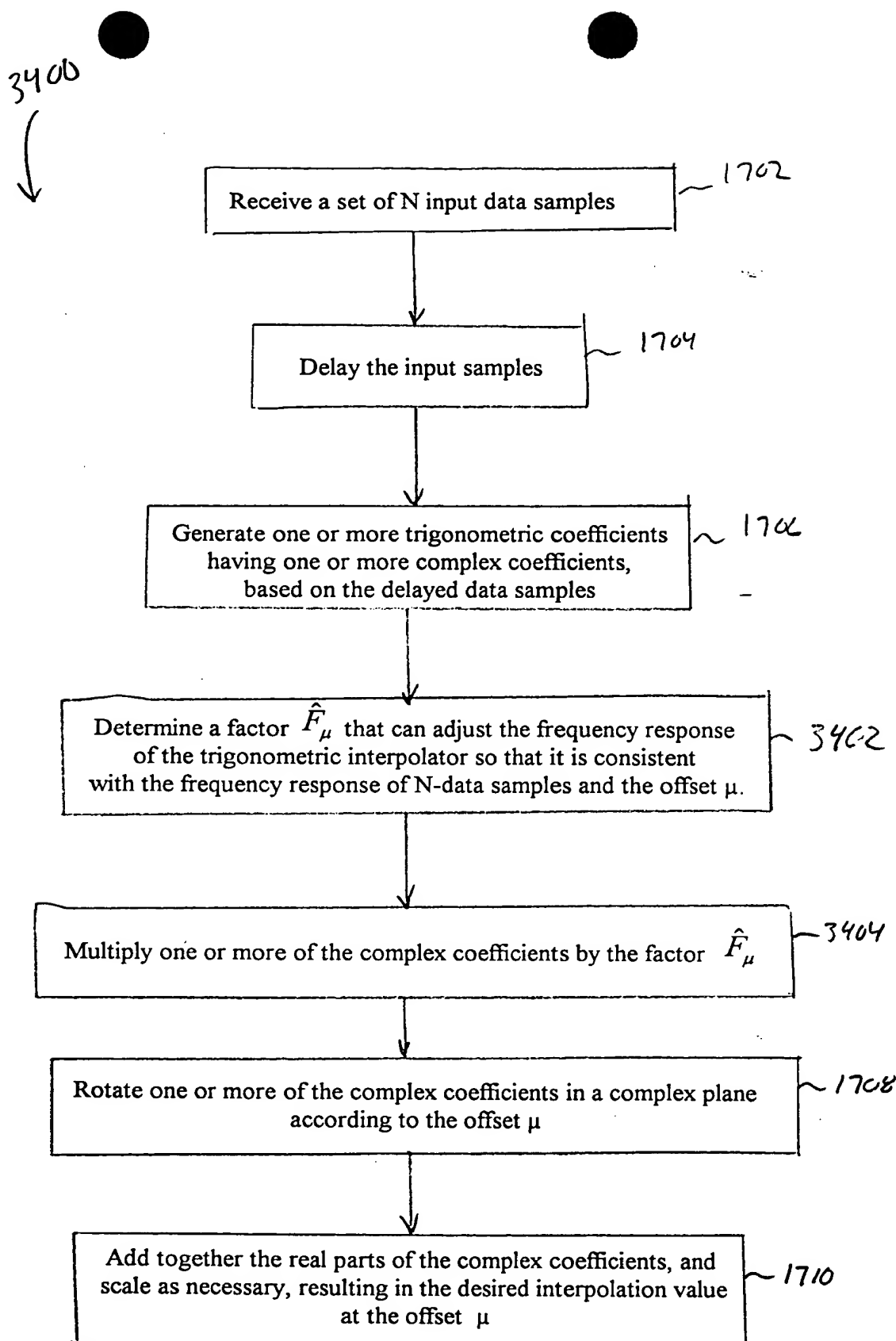


FIG. 33: Signal with two samples/symbol and 40% excess bandwidth.



00000000000000000000000000000000

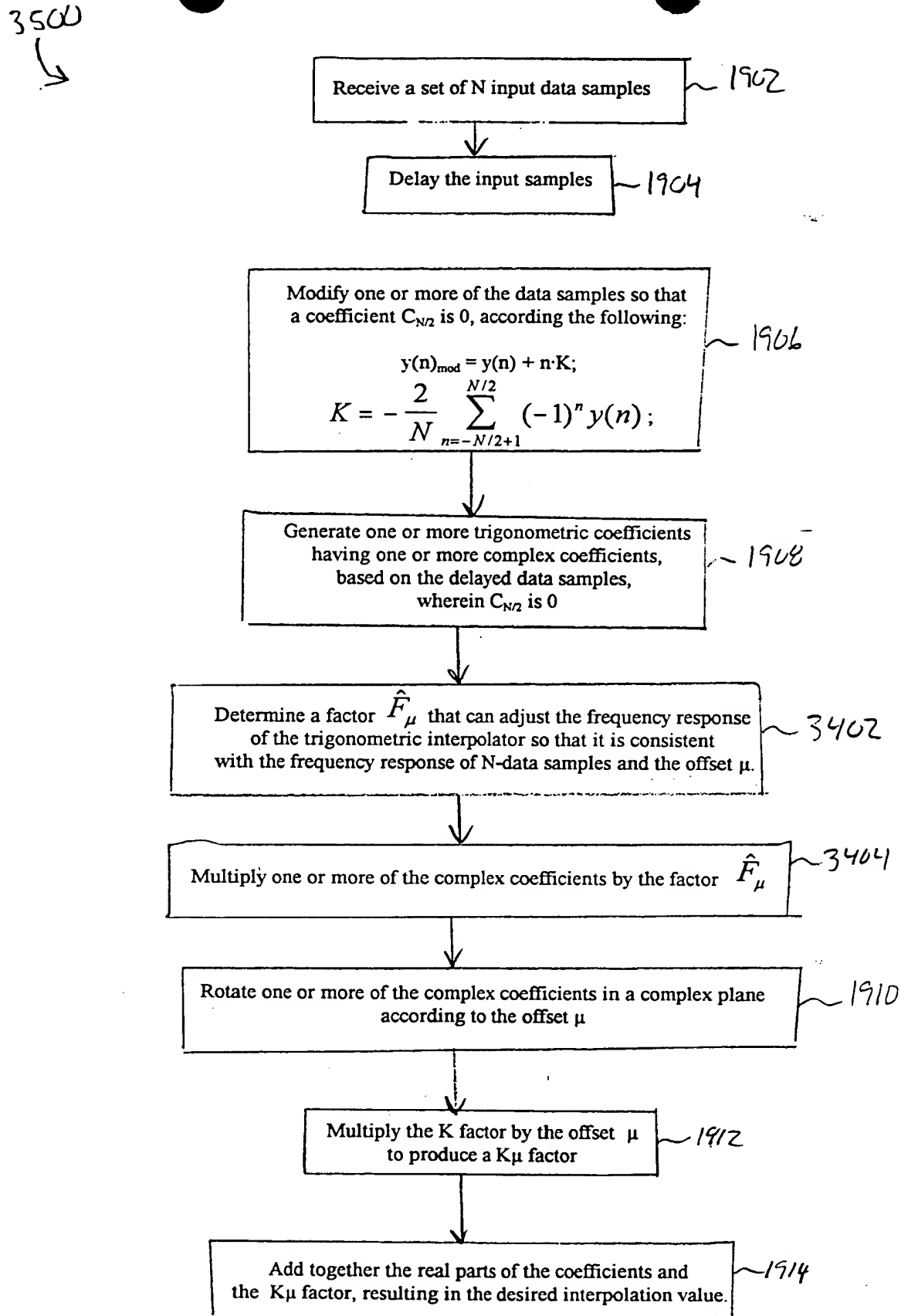


FIG. 35

3600

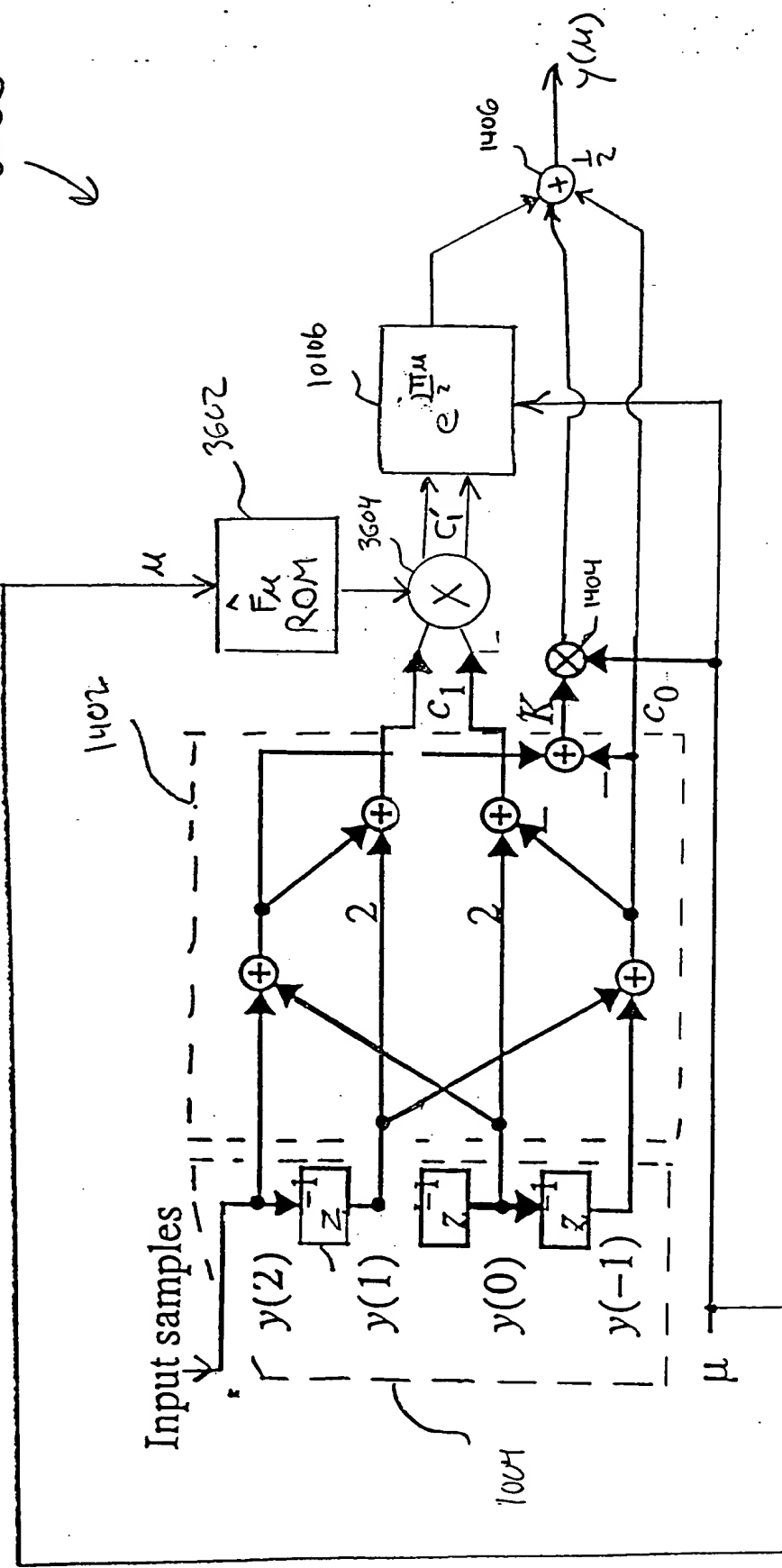


Fig. 36 The optimized structure for $N=4$.

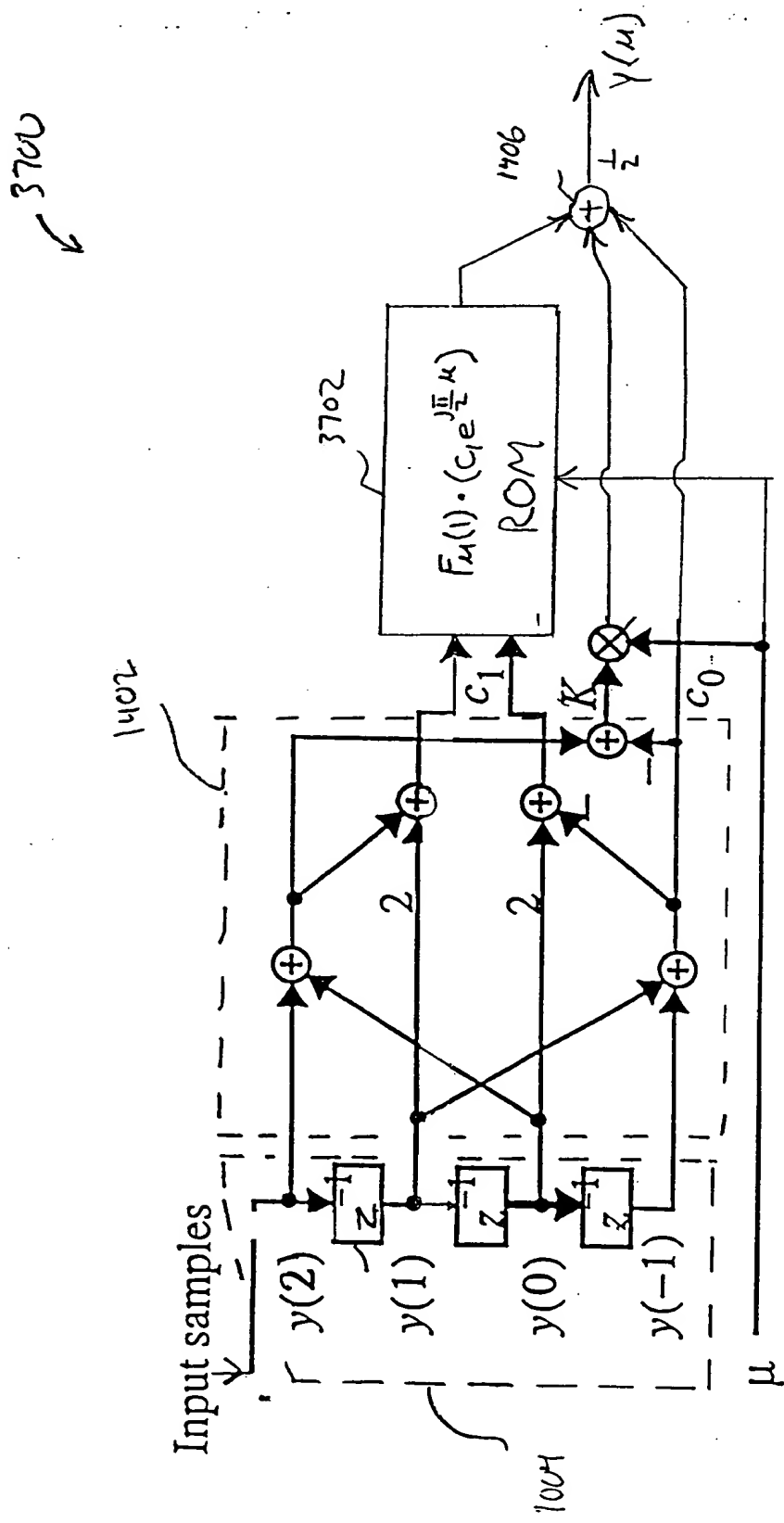


FIG.37 : The optimized structure for $N=4$.

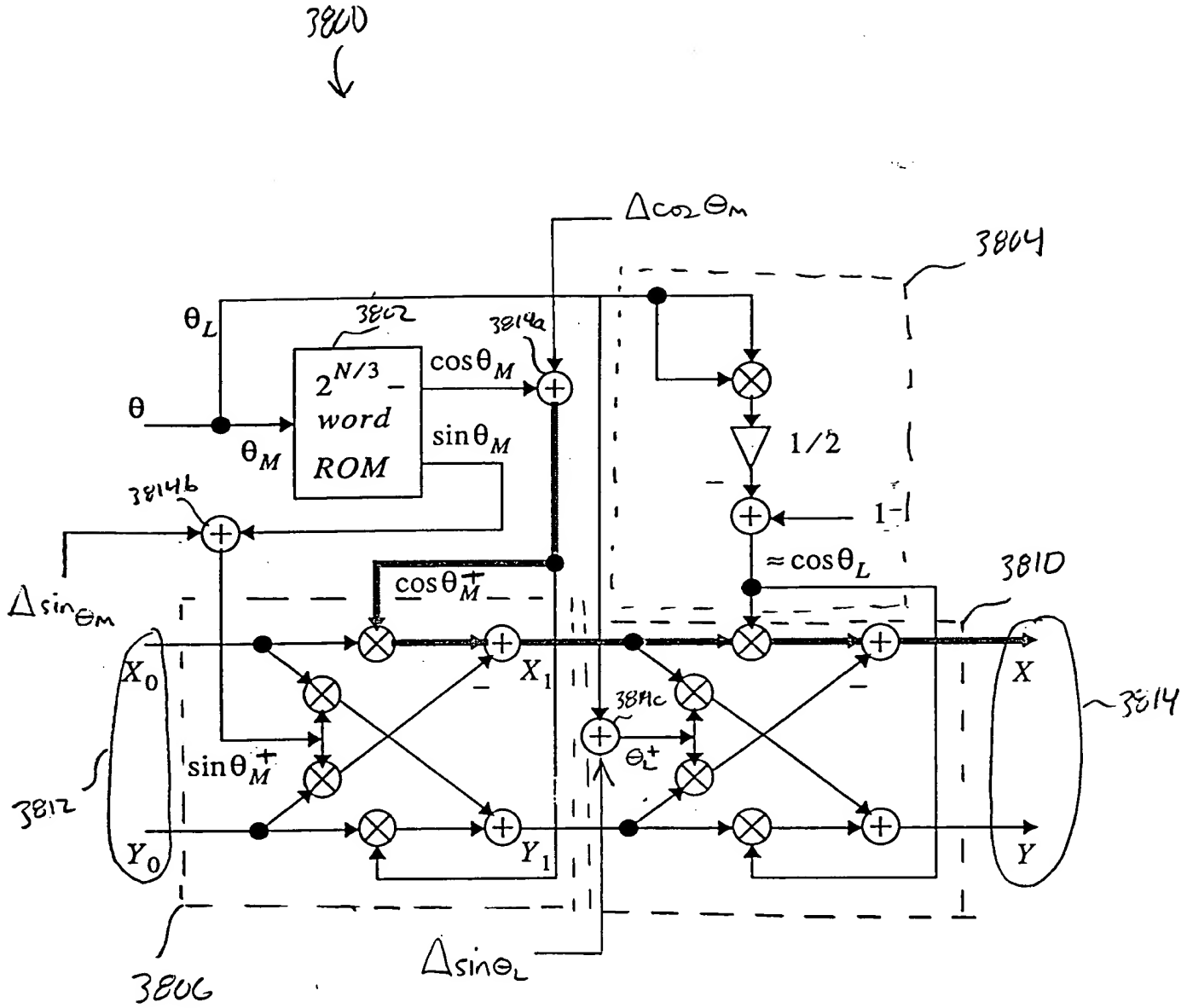


FIG. 38

3906

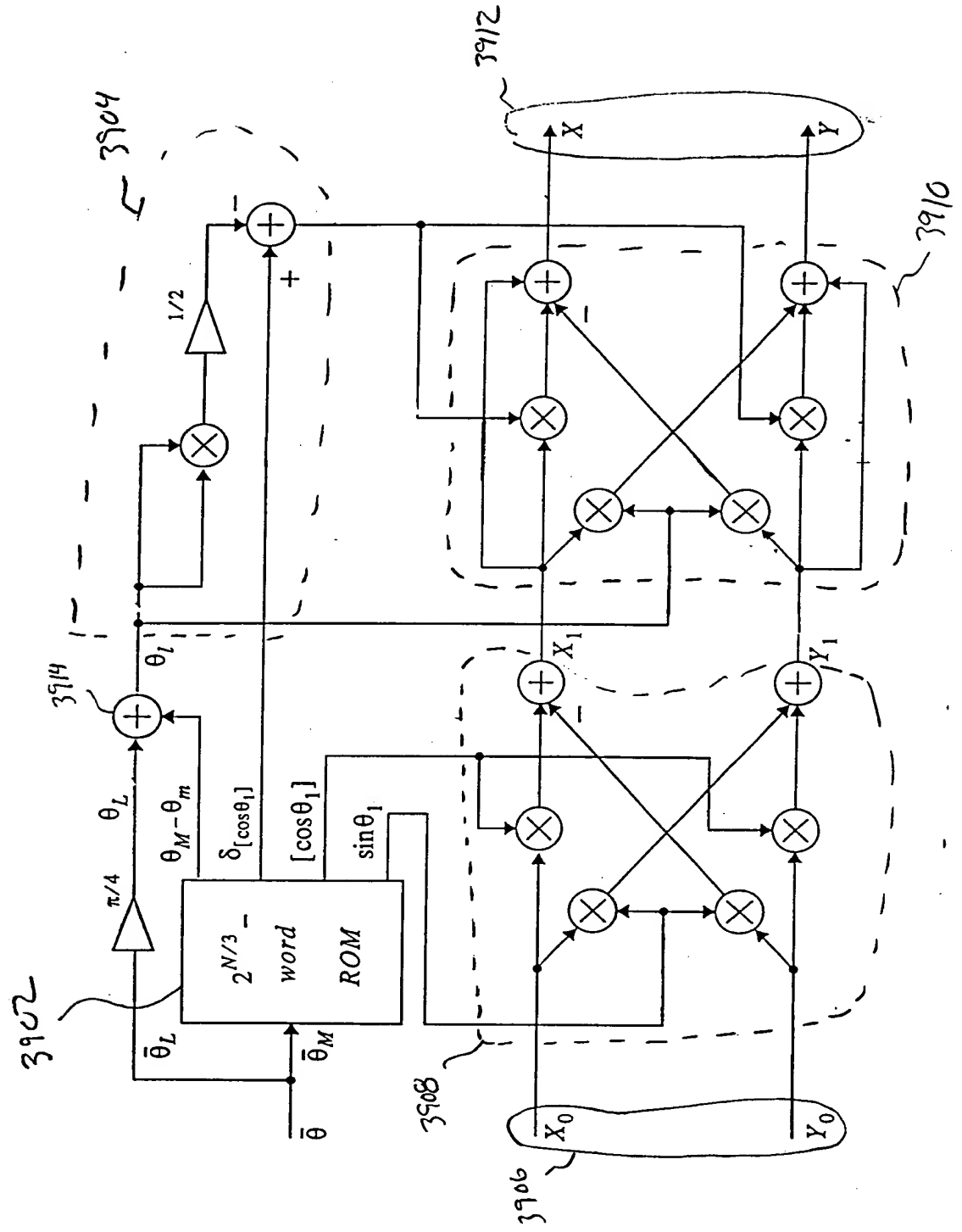


FIG. 39

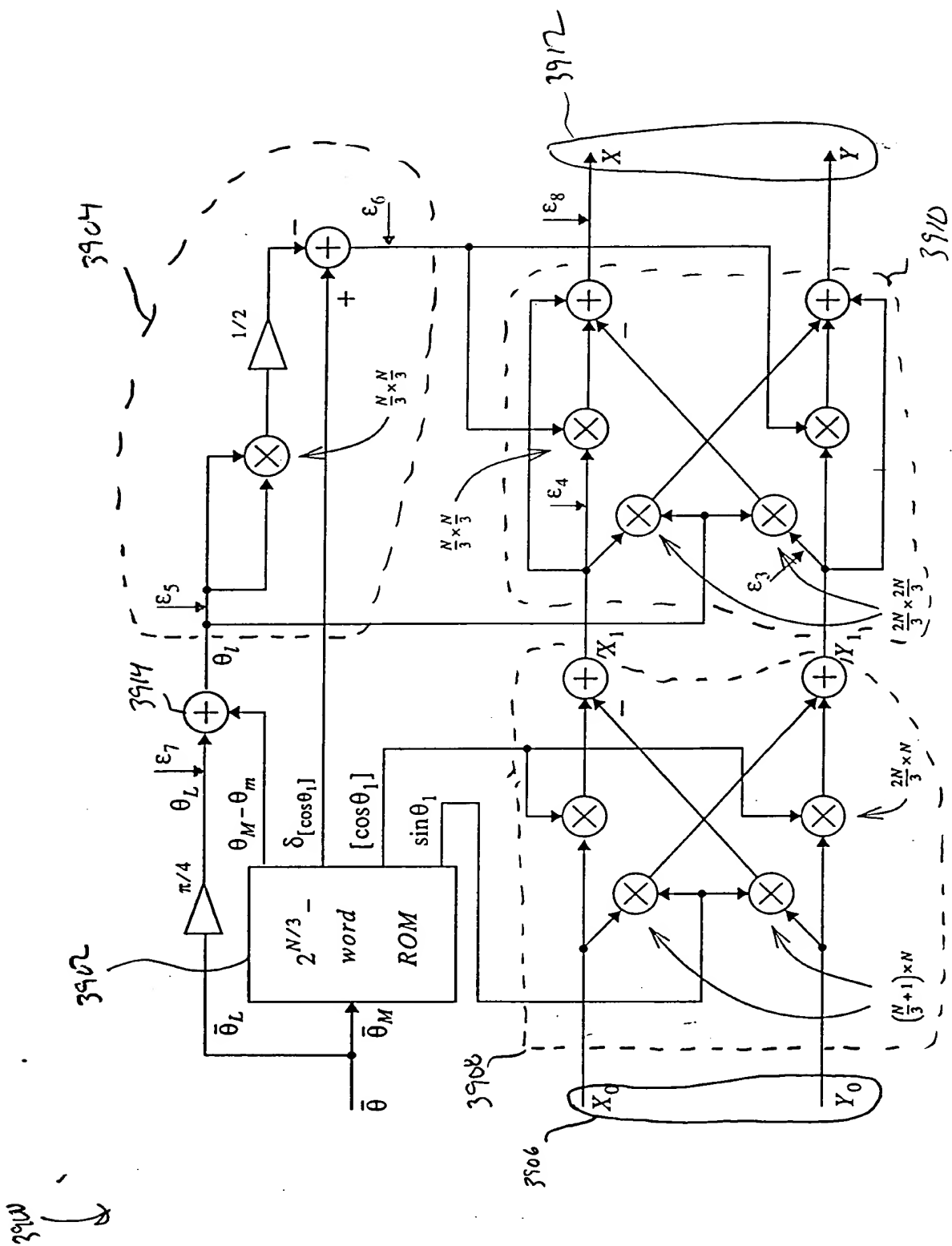


Fig. 40

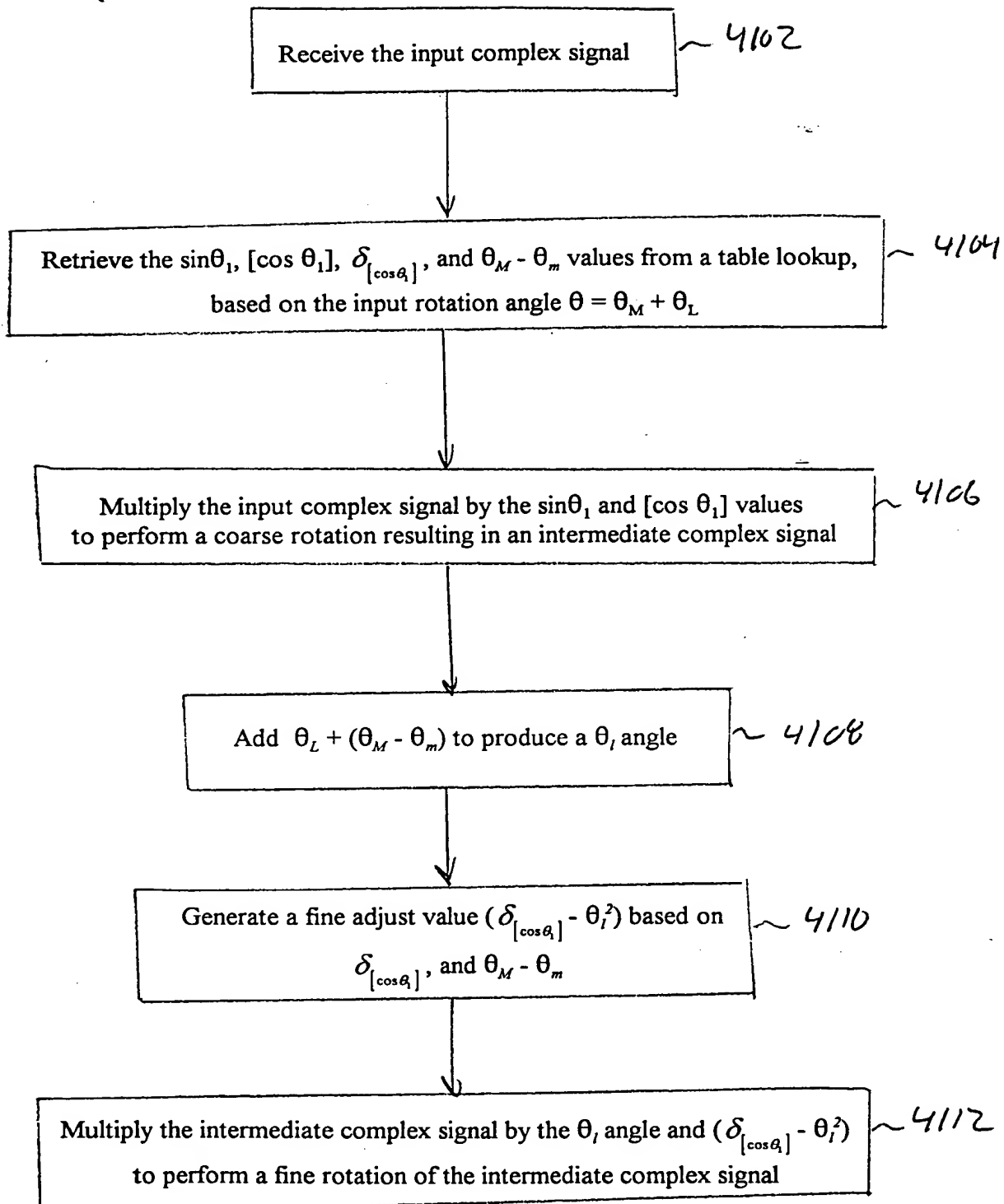


FIG. 41

3900

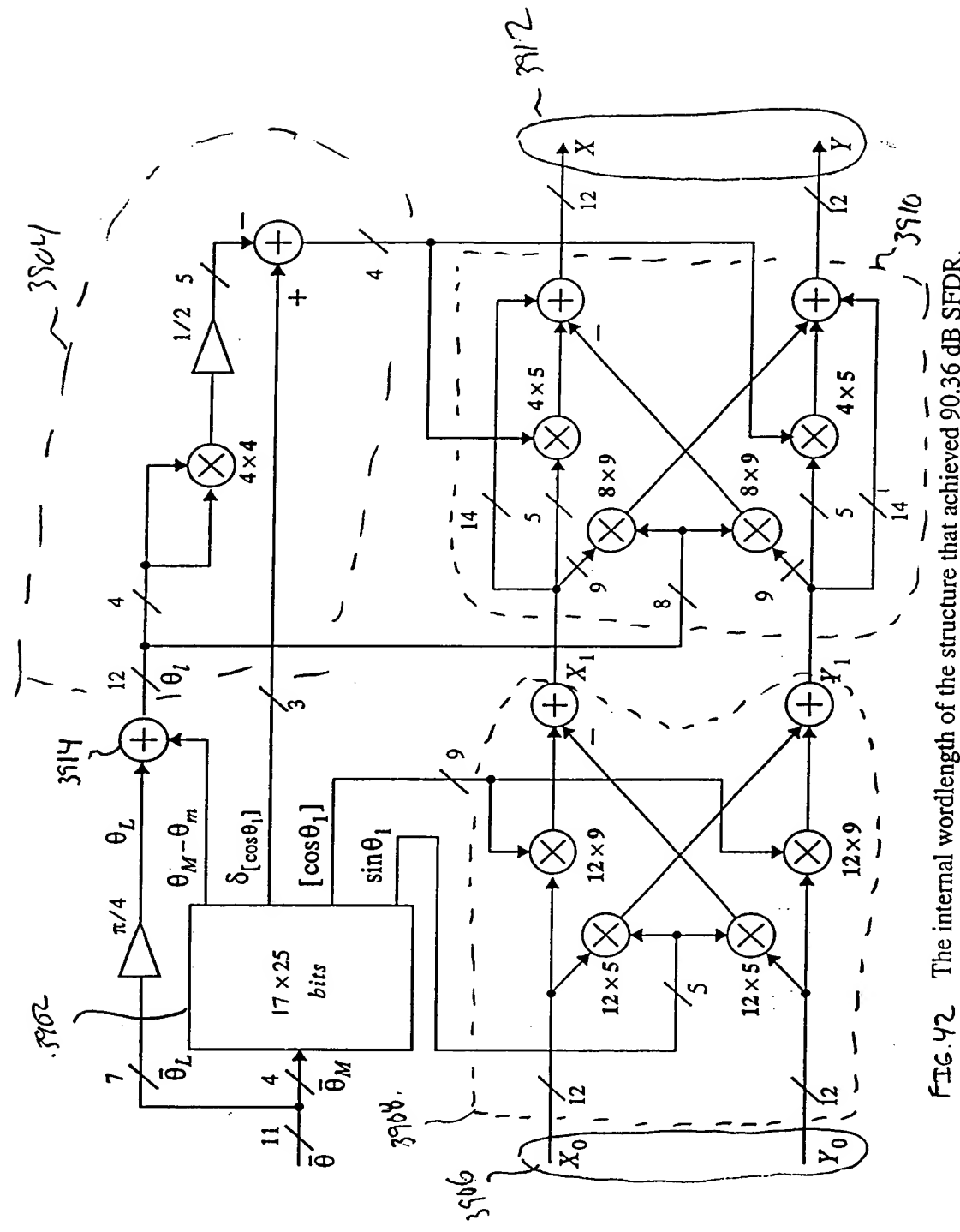


FIG. 42 The internal wordlength of the structure that achieved 90.36 dB SFDR.

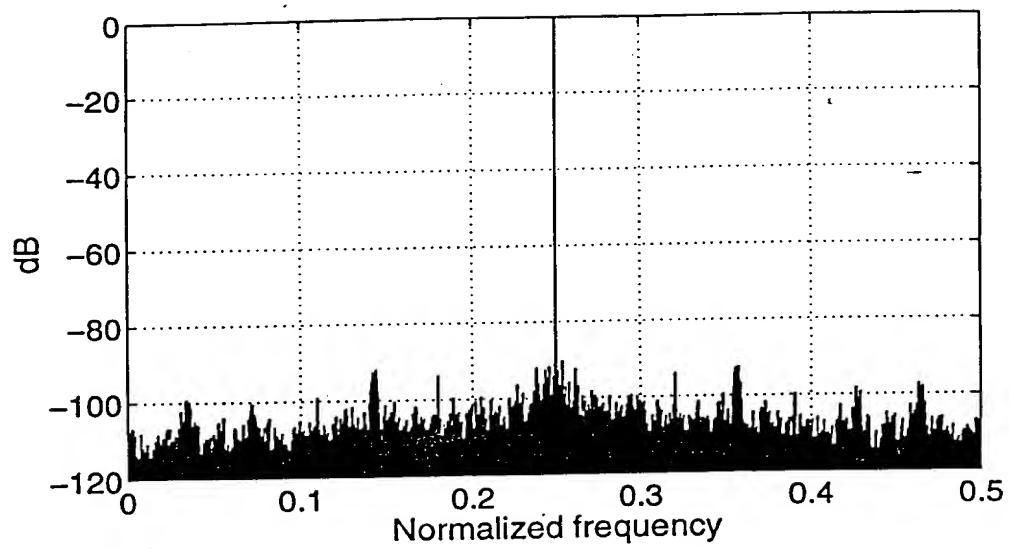


FIG. 43 Output spectrum showing 90.36 dB SFDR.

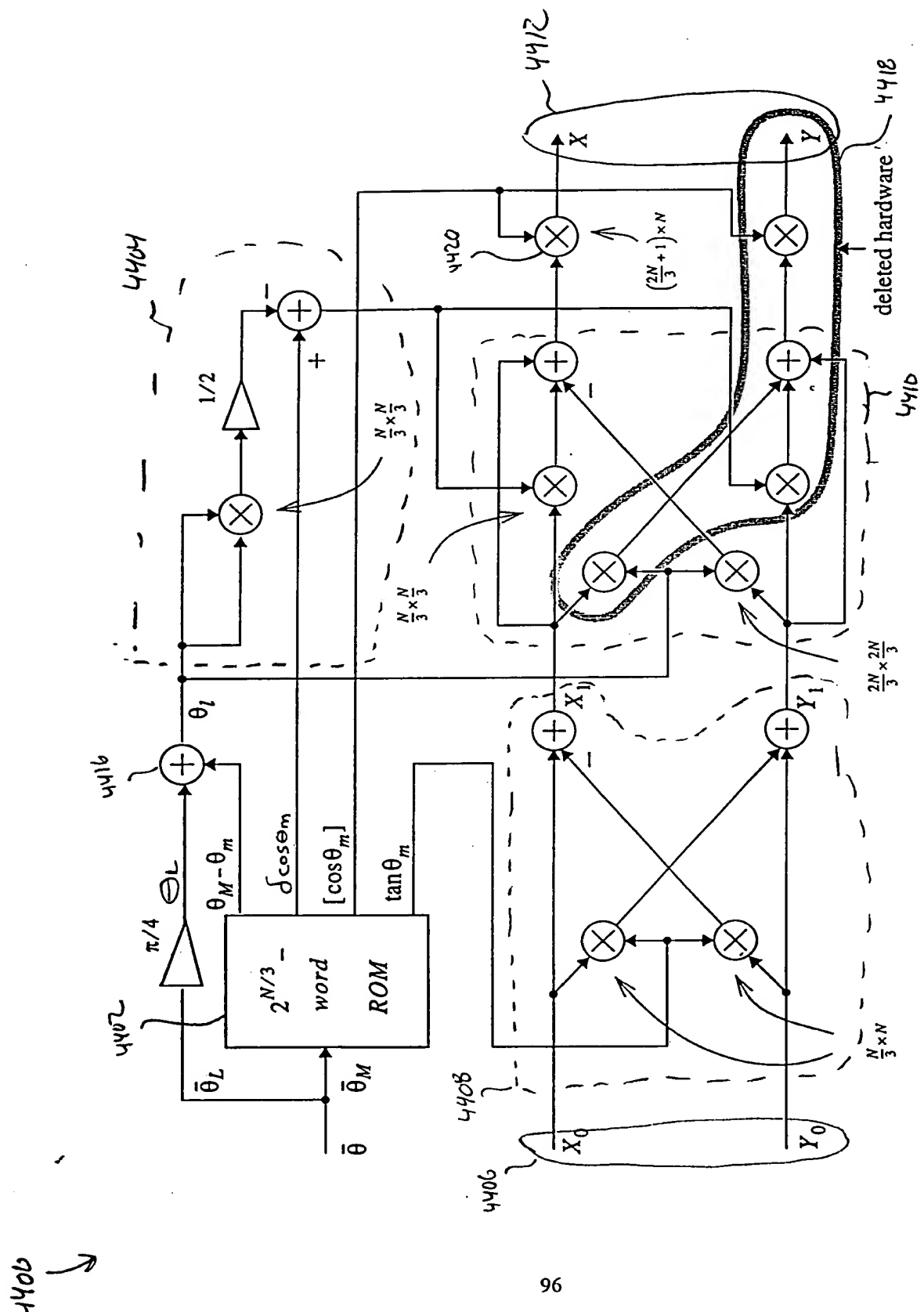
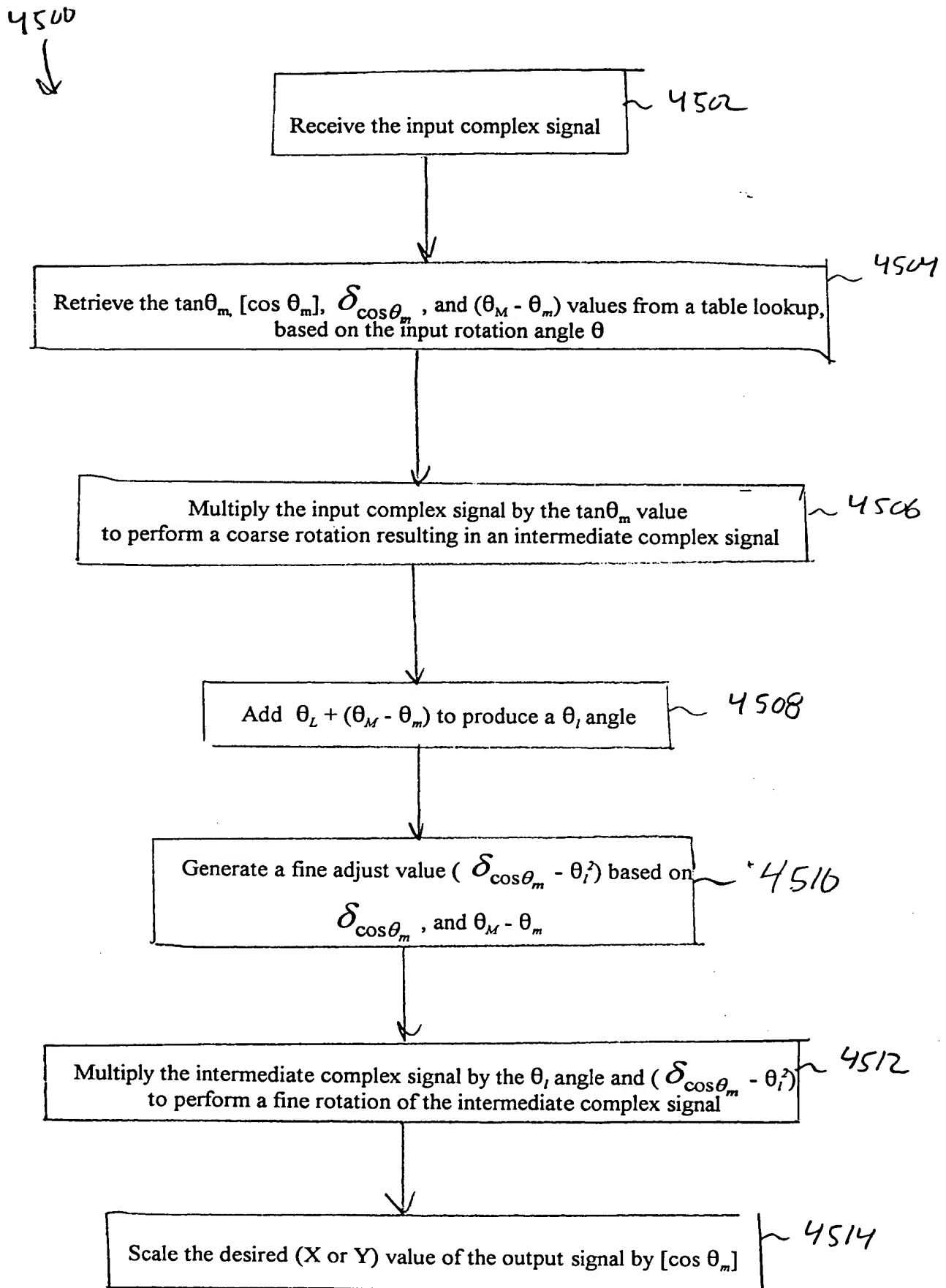


FIG. 44 A modified architecture when only one output is needed.



4600

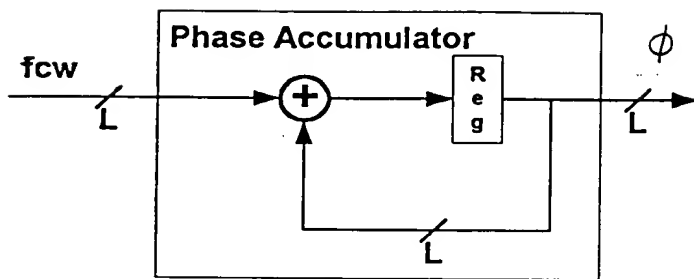
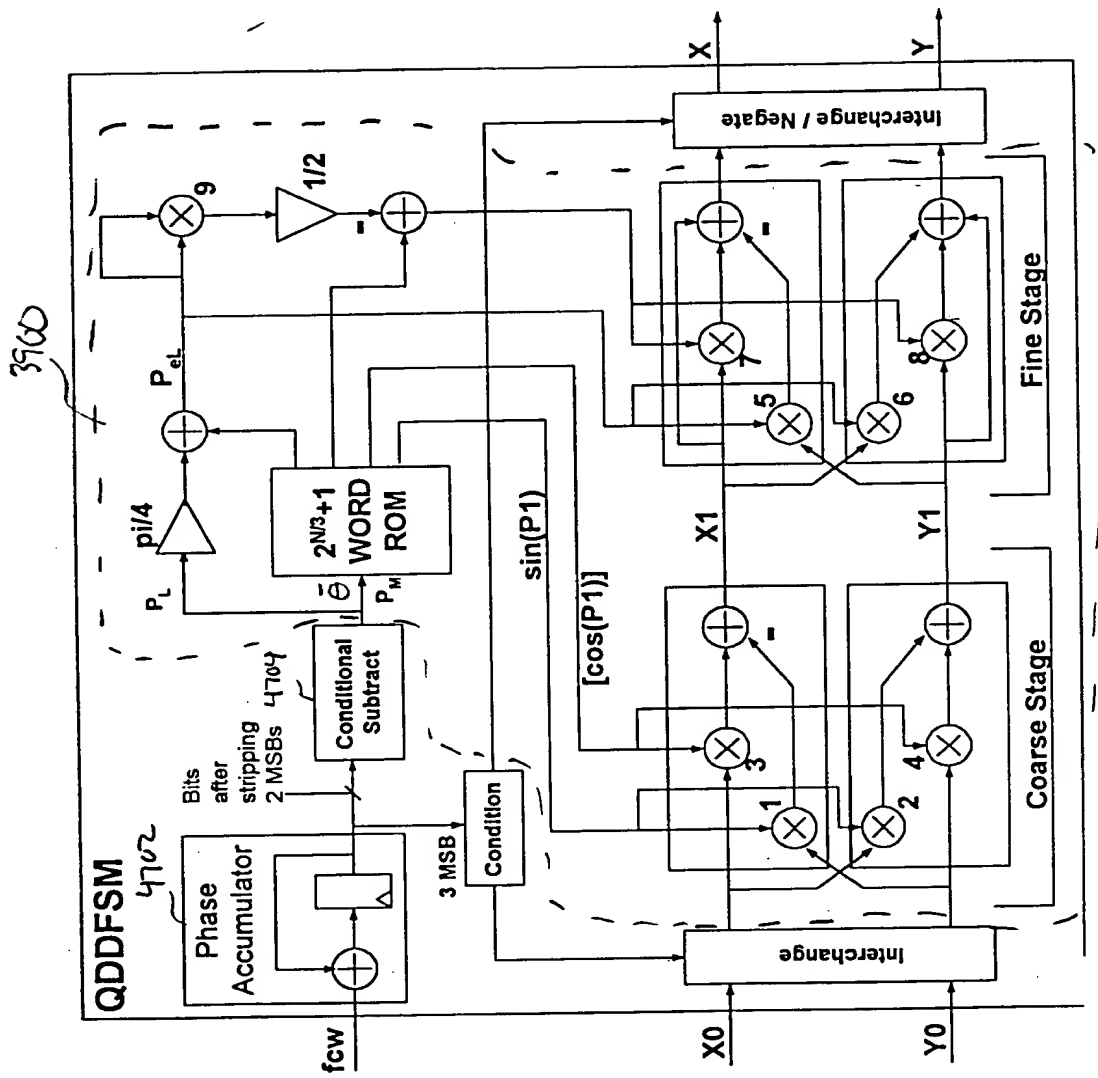
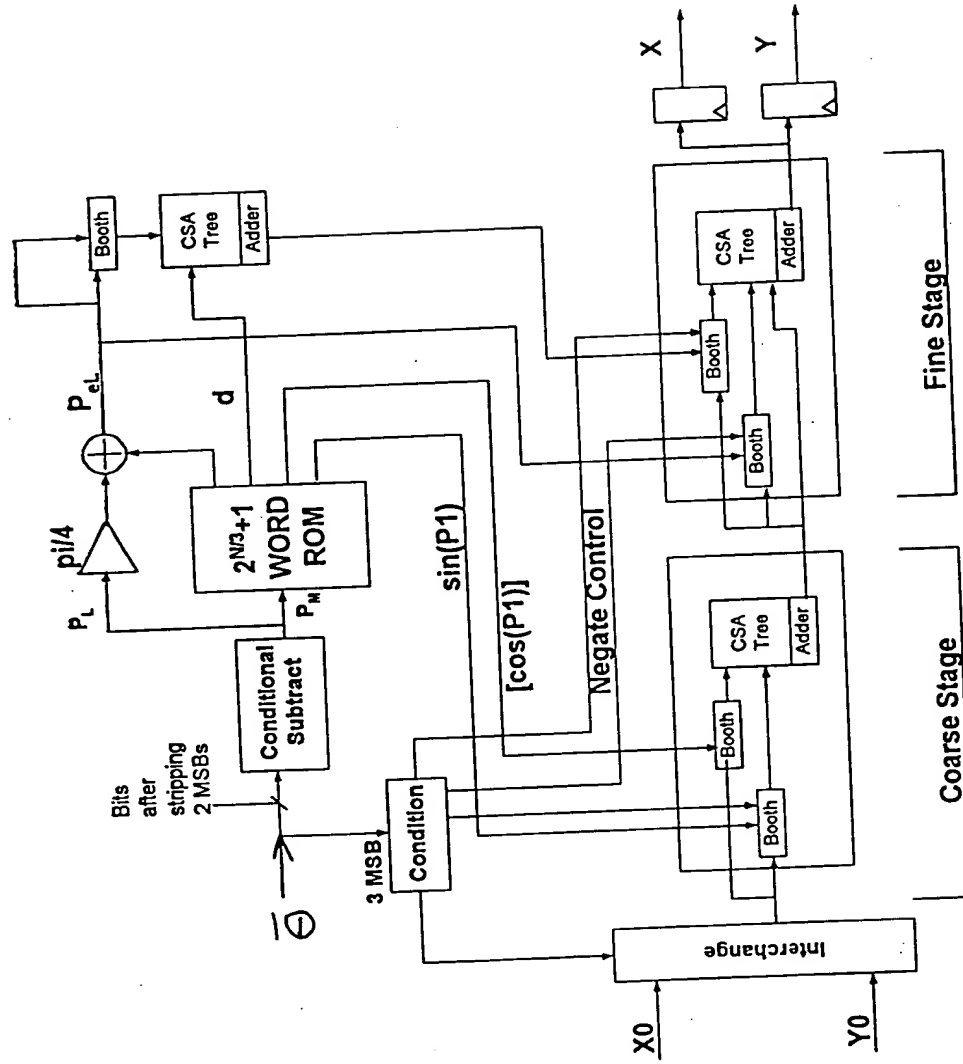


FIG. 46

where the adder is an overflowing
accumulator.



FTC 47



Upward

Fig. 48

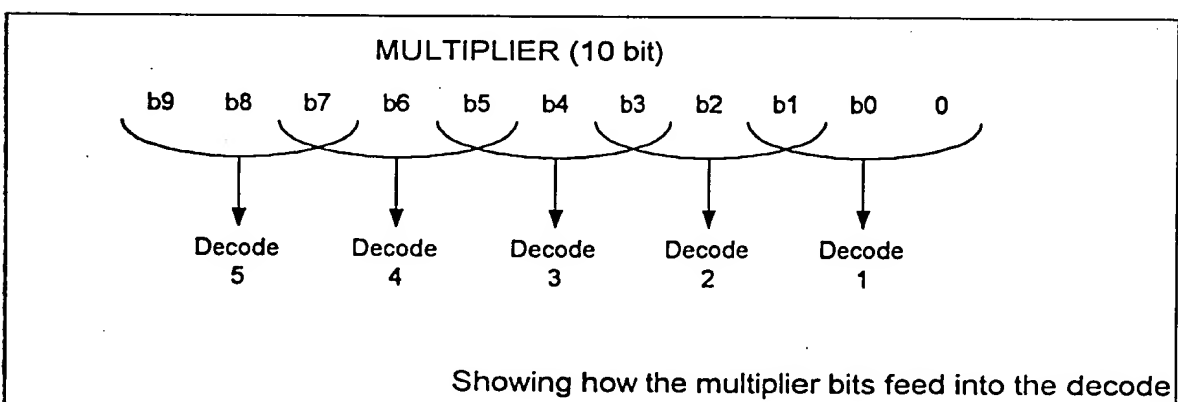
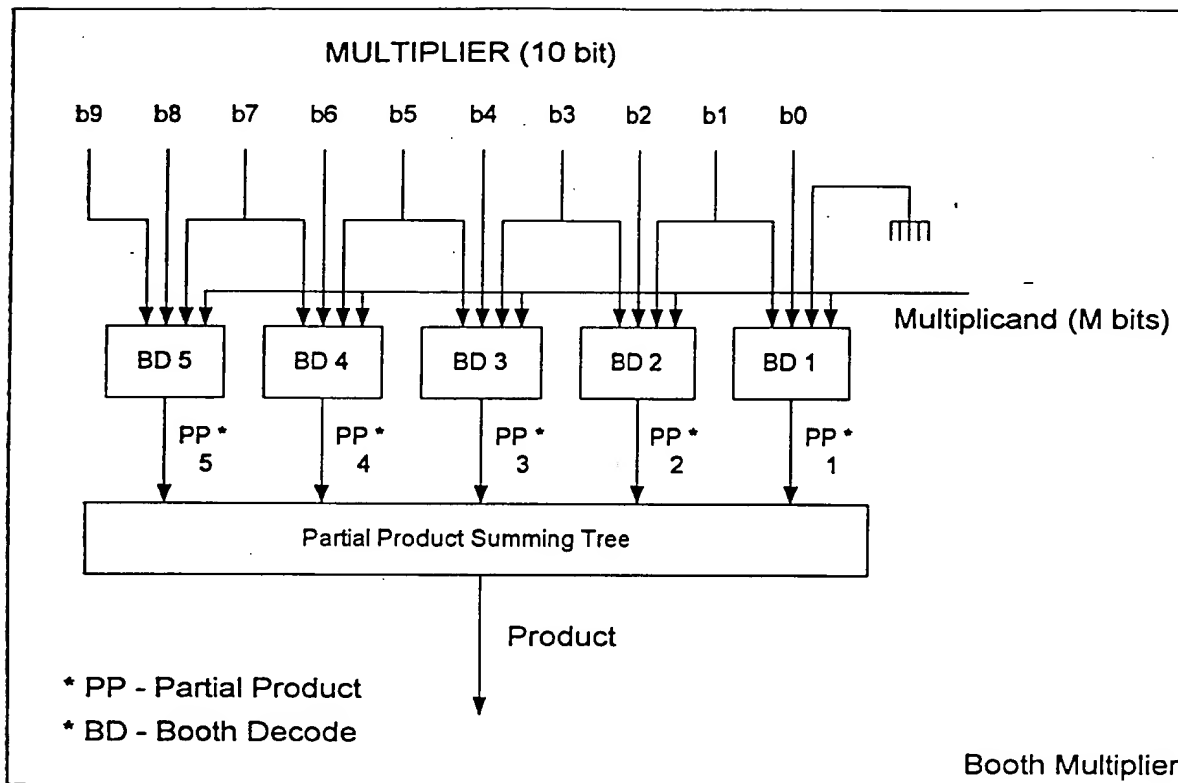


FIG. 49

5000

Original Booth Table

5062

b2 b1 b0 PP

| | | | |
|---|---|---|-----|
| 0 | 0 | 0 | 0*A |
| 0 | 0 | 1 | 1*A |
| 0 | 1 | 0 | 1*A |
| 0 | 1 | 1 | 2*A |

| | | | |
|---|---|---|---------|
| 1 | 0 | 0 | -2^*A |
| 1 | 0 | 1 | -1^*A |
| 1 | 1 | 0 | -1^*A |
| 1 | 1 | 1 | 0^*A |

5100

Negating Booth Table

- 5102

b2 b1 b0 PP

| | | | |
|---|---|---|---------|
| 0 | 0 | 0 | 0^*A |
| 0 | 0 | 1 | -1^*A |
| 0 | 1 | 0 | -1^*A |
| 0 | 1 | 1 | -2^*A |

| | | | |
|---|---|---|--------|
| 1 | 0 | 0 | 2^*A |
| 1 | 0 | 1 | 1^*A |
| 1 | 1 | 0 | 1^*A |
| 1 | 1 | 1 | 0^*A |

FIG. 50

FIG. 51

5266

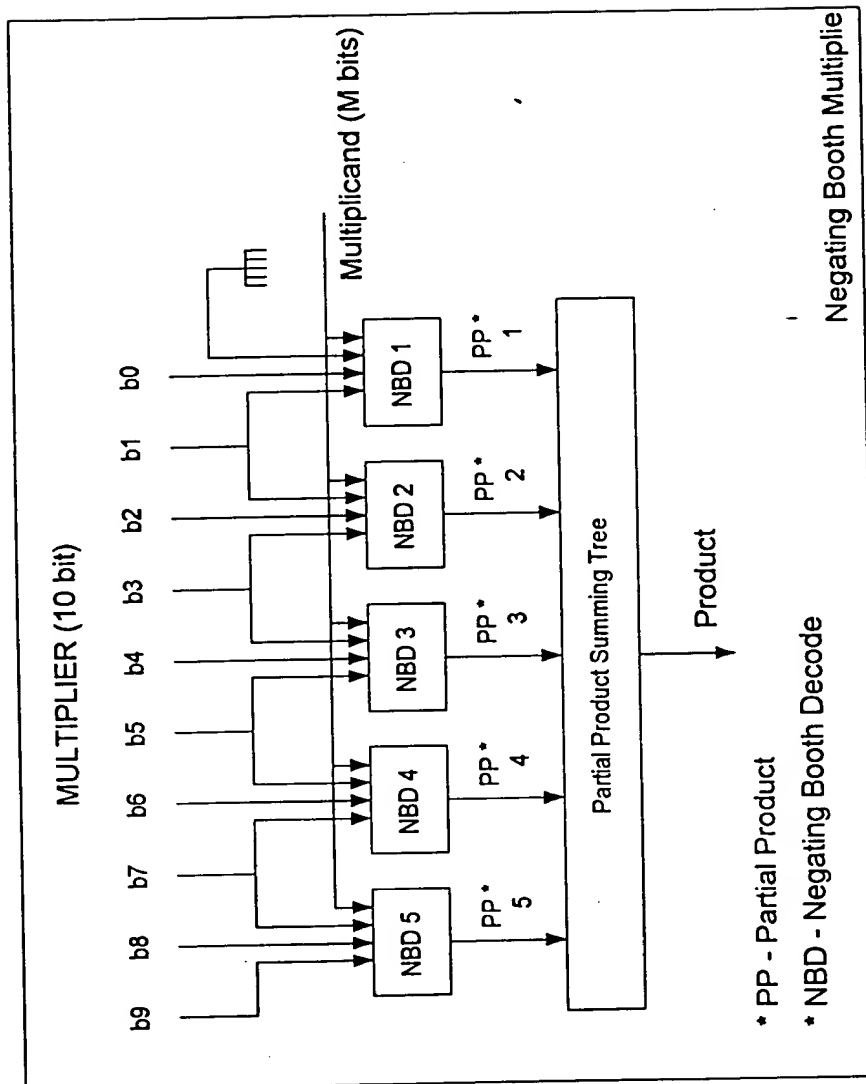
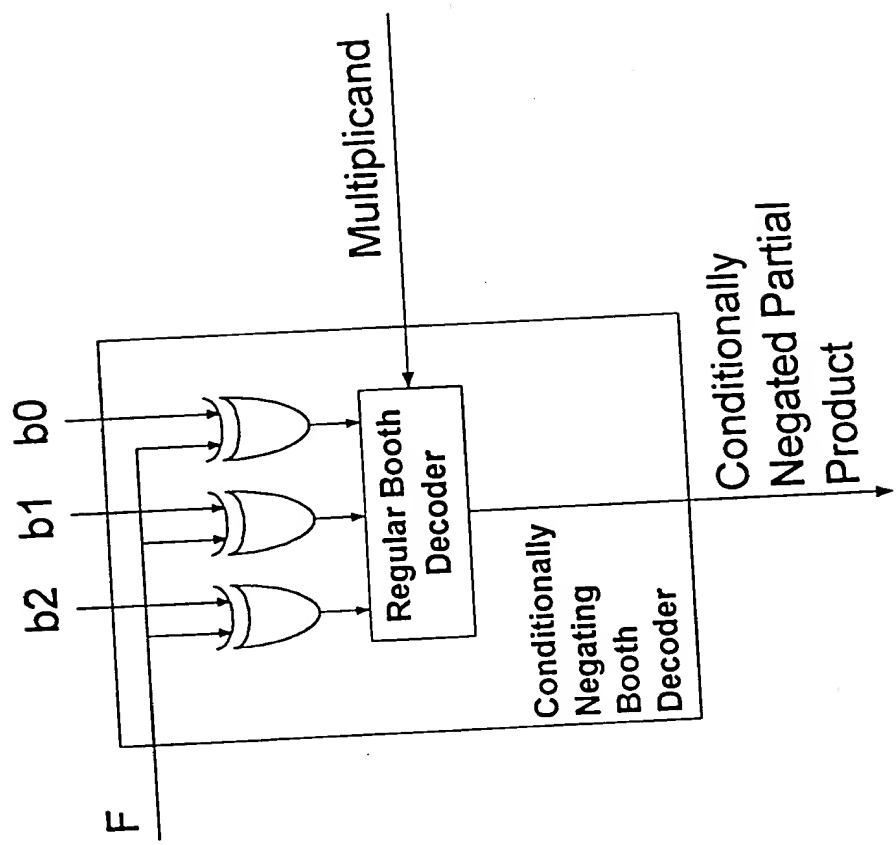


FIG. 52



5300

FIG. 53

卷之三

54cb

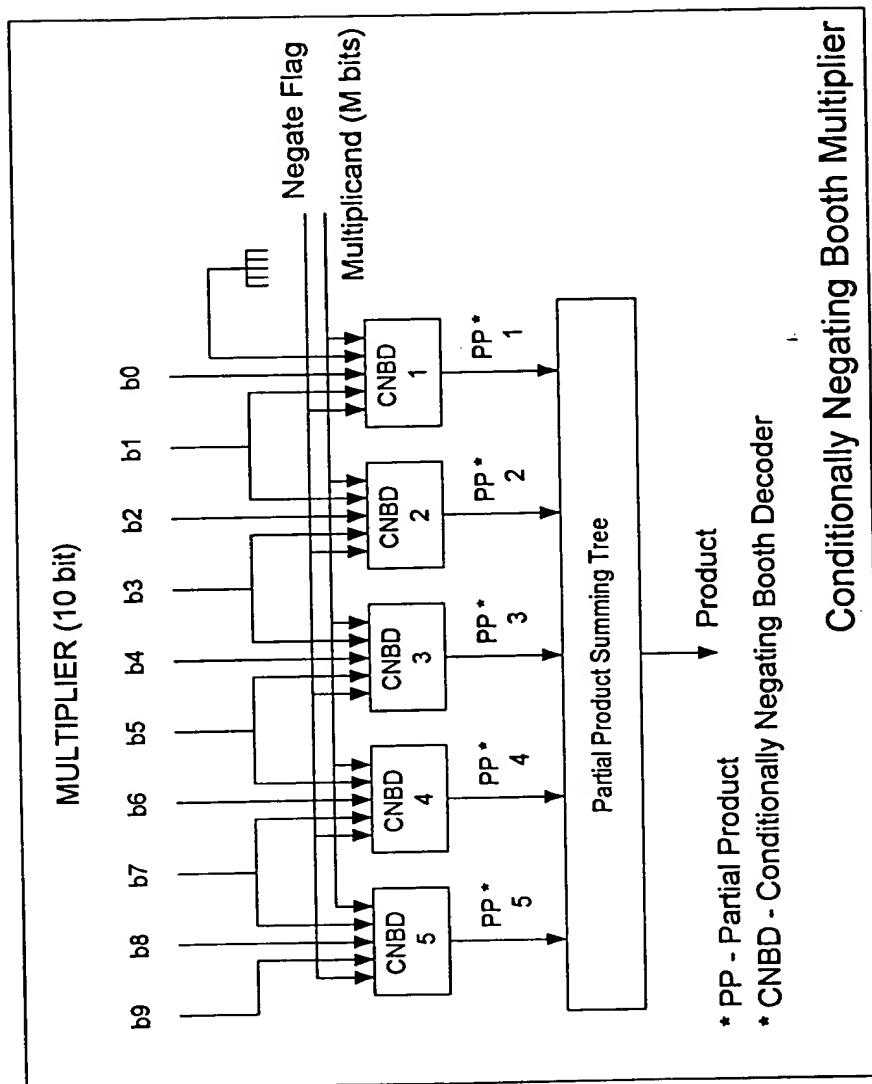


FIG. 54

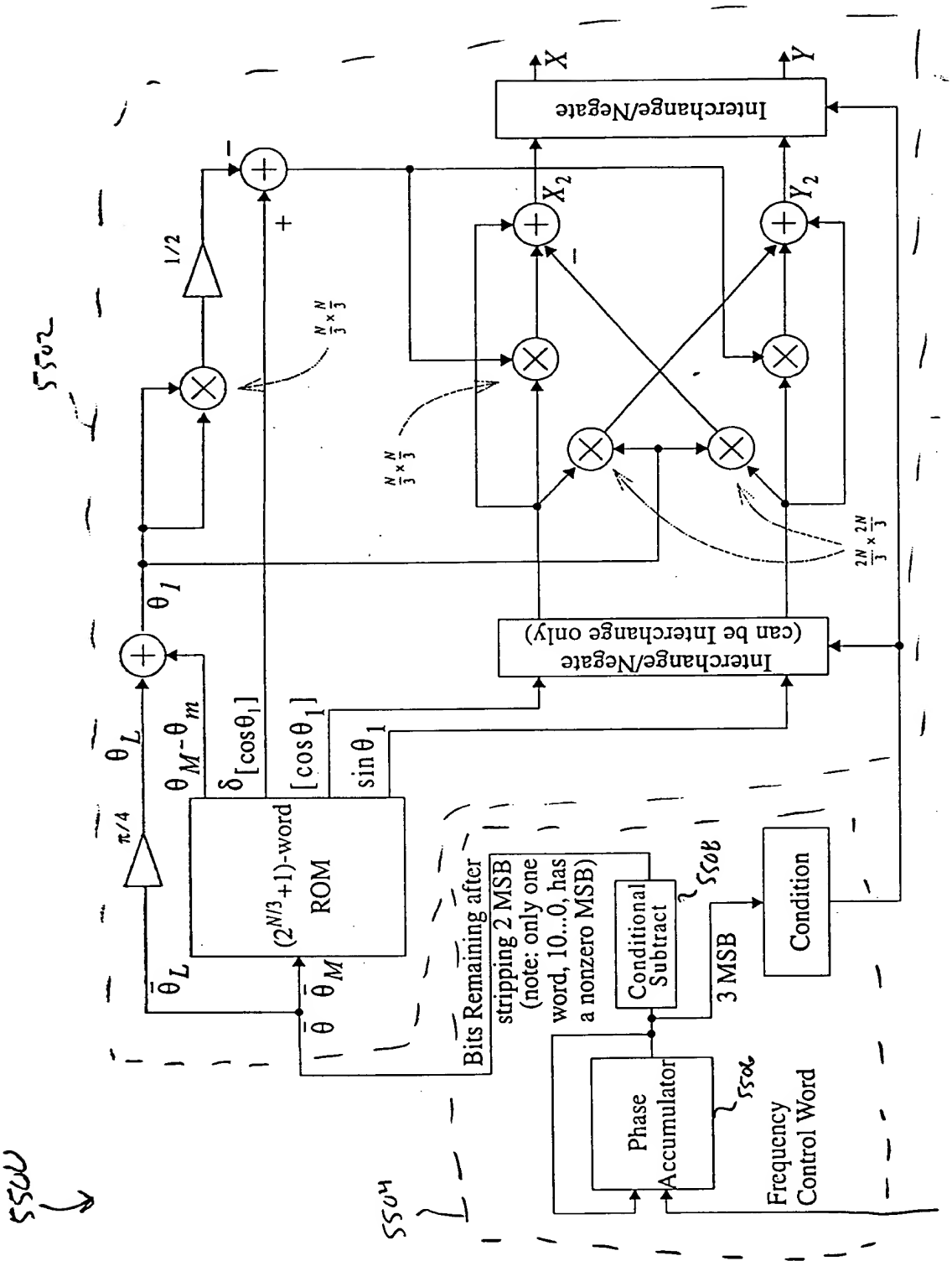


Fig. 55 Angle Rotator Configured as a Quadrature Direct Digital Synthesizer (QDDS).

5600

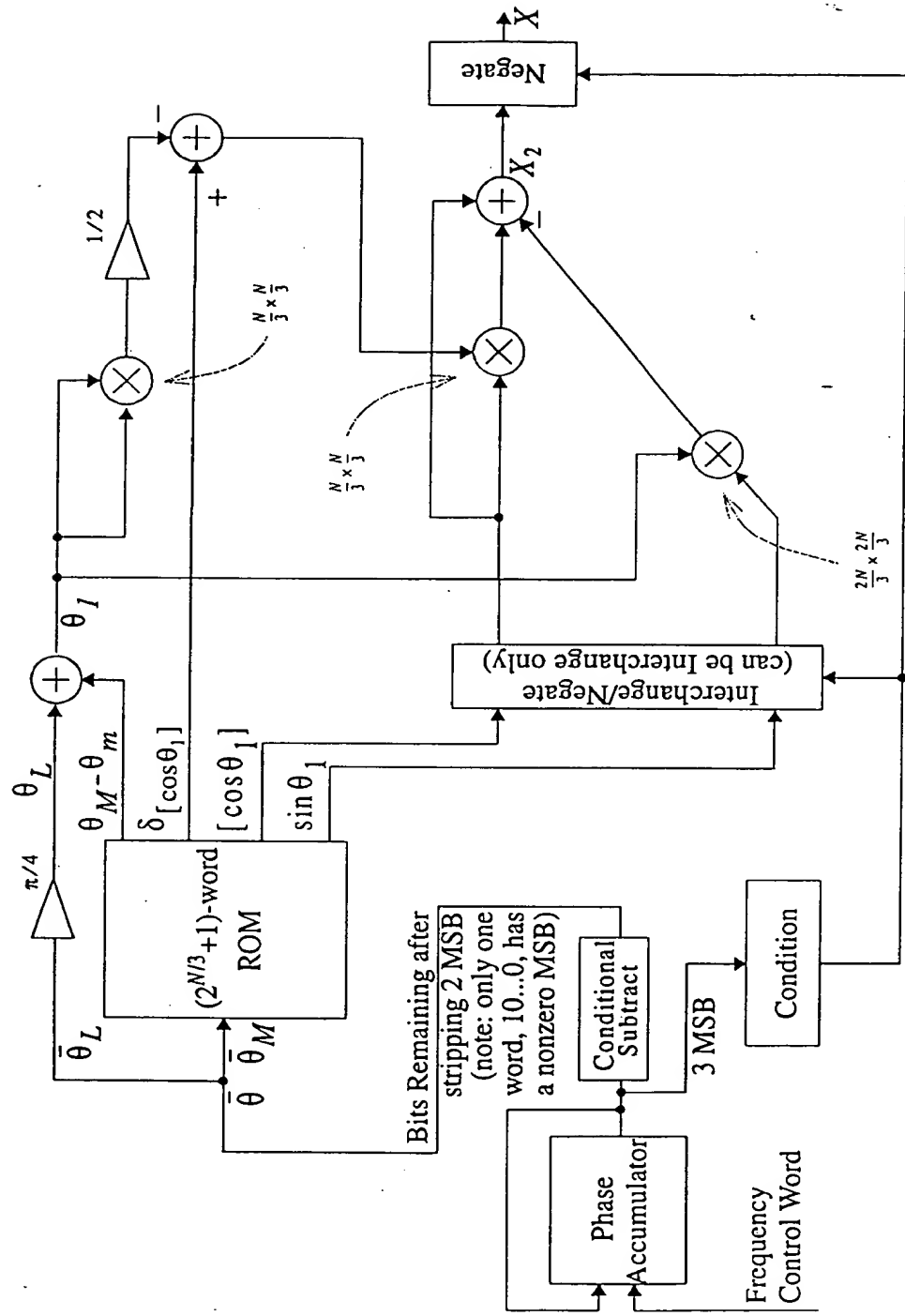
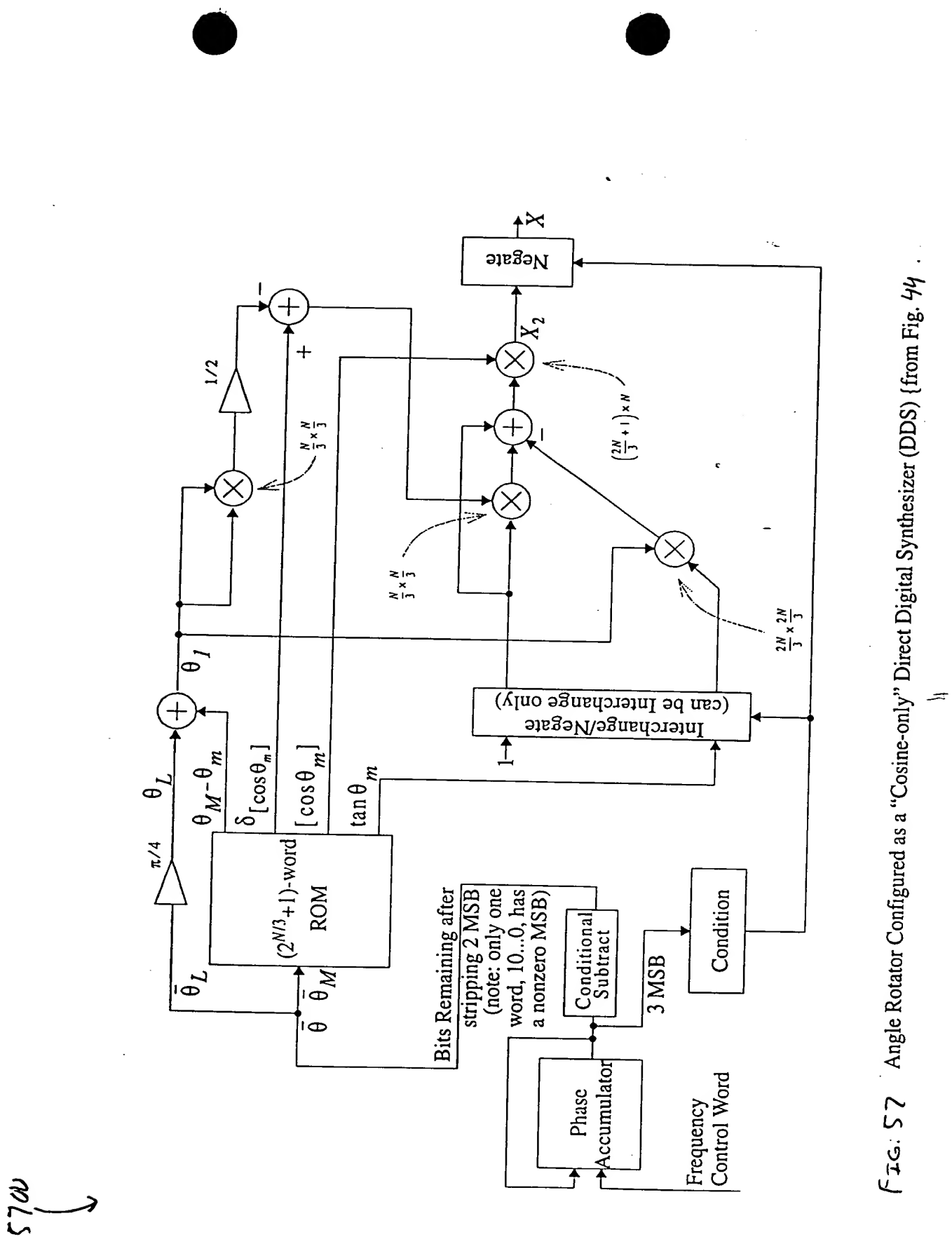


Fig. 56 Angle Rotator Configured as a "Cosine-only" Direct Digital Synthesizer (DDS) [from Fig. 37].



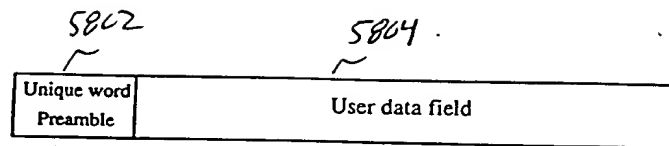


FIG. 58: Common packet format.

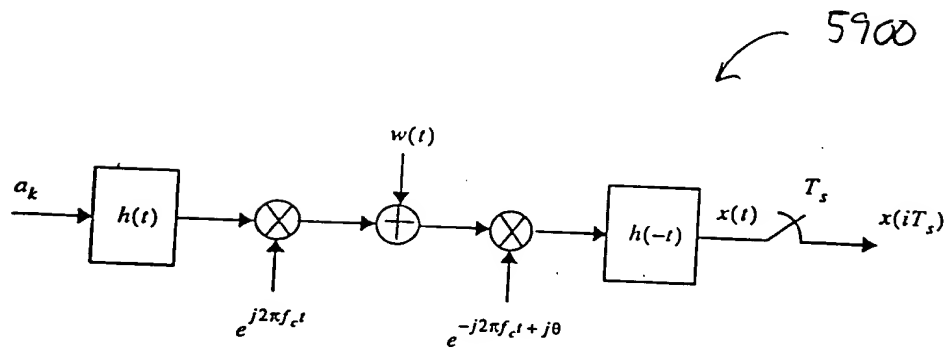


FIG. 59: The simplified system model.

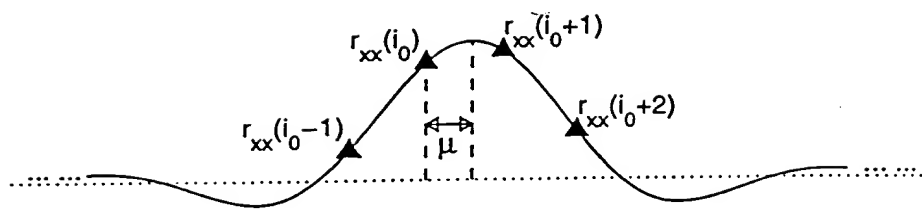


FIG. 60 Mean values of the preamble correlator output, for $\theta = 0$.

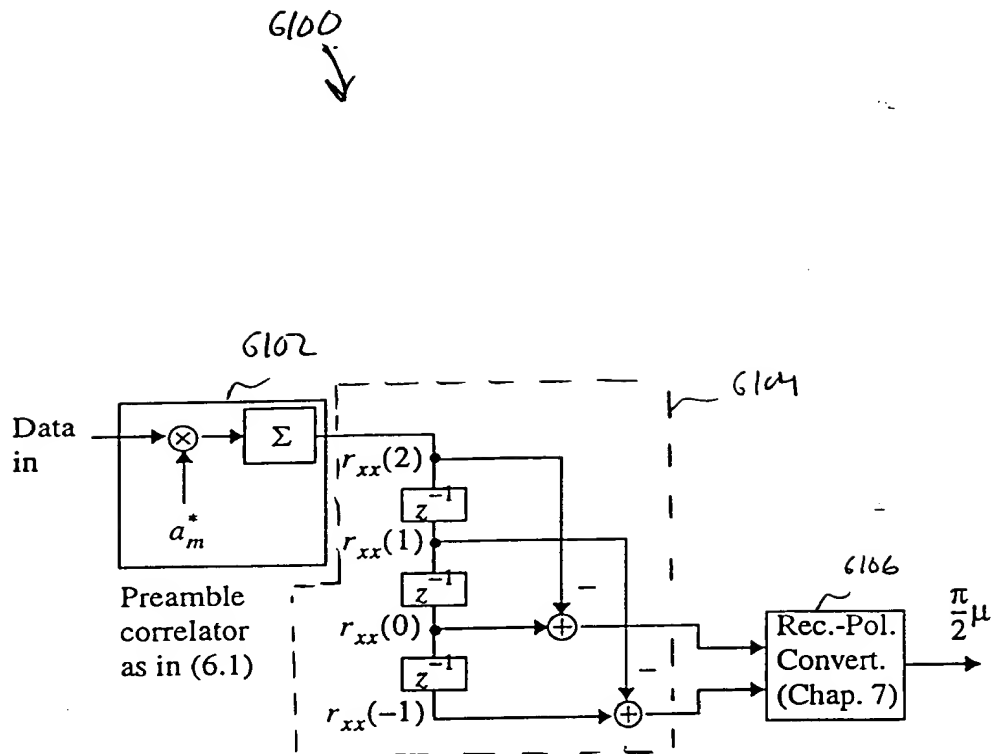


FIG. 61: Preliminary symbol-timing estimation structure.

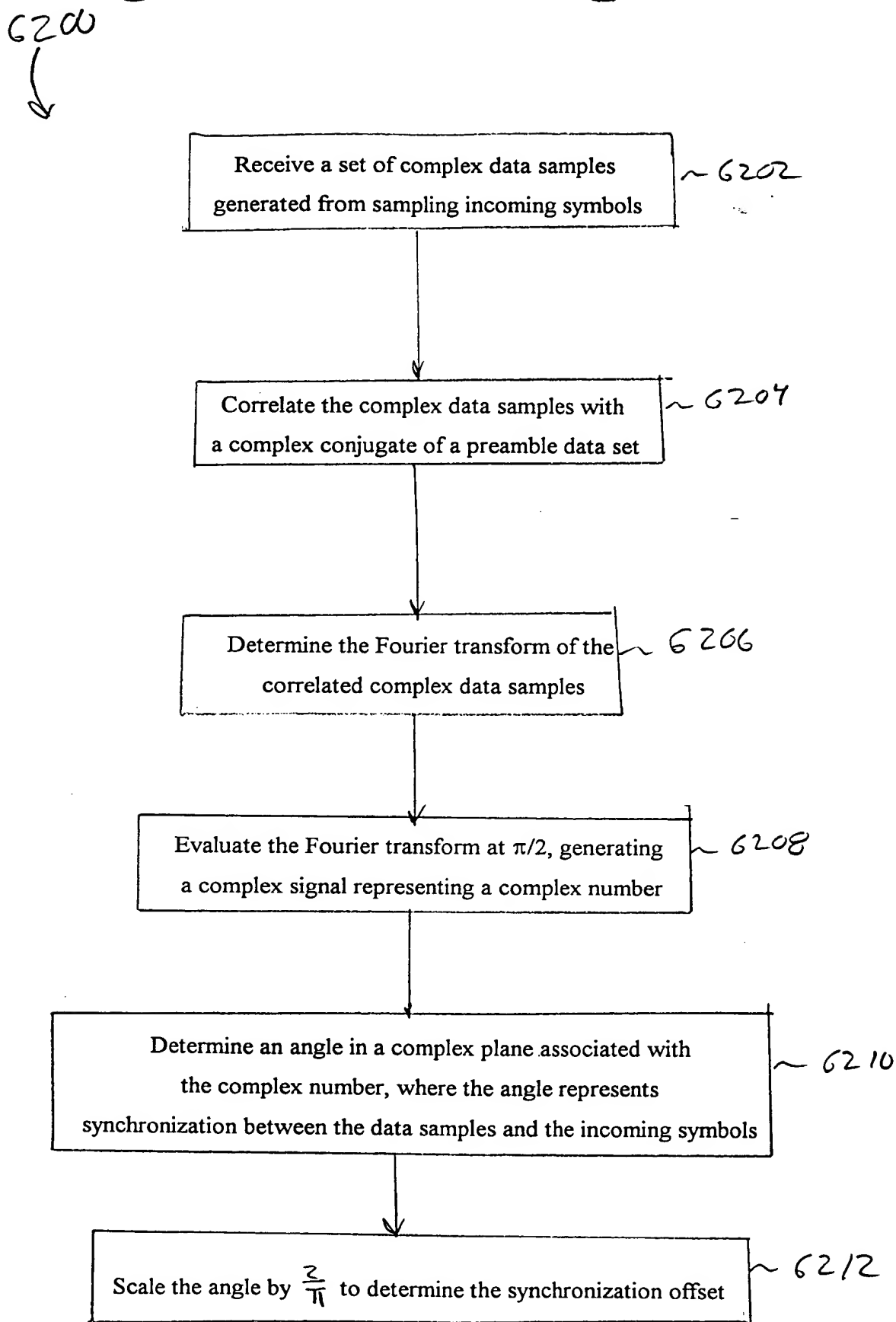


FIG. 62

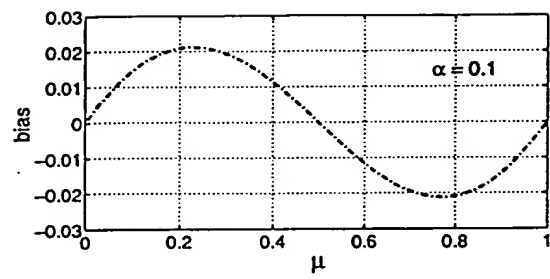


FIG. 63 Bias due to truncation.

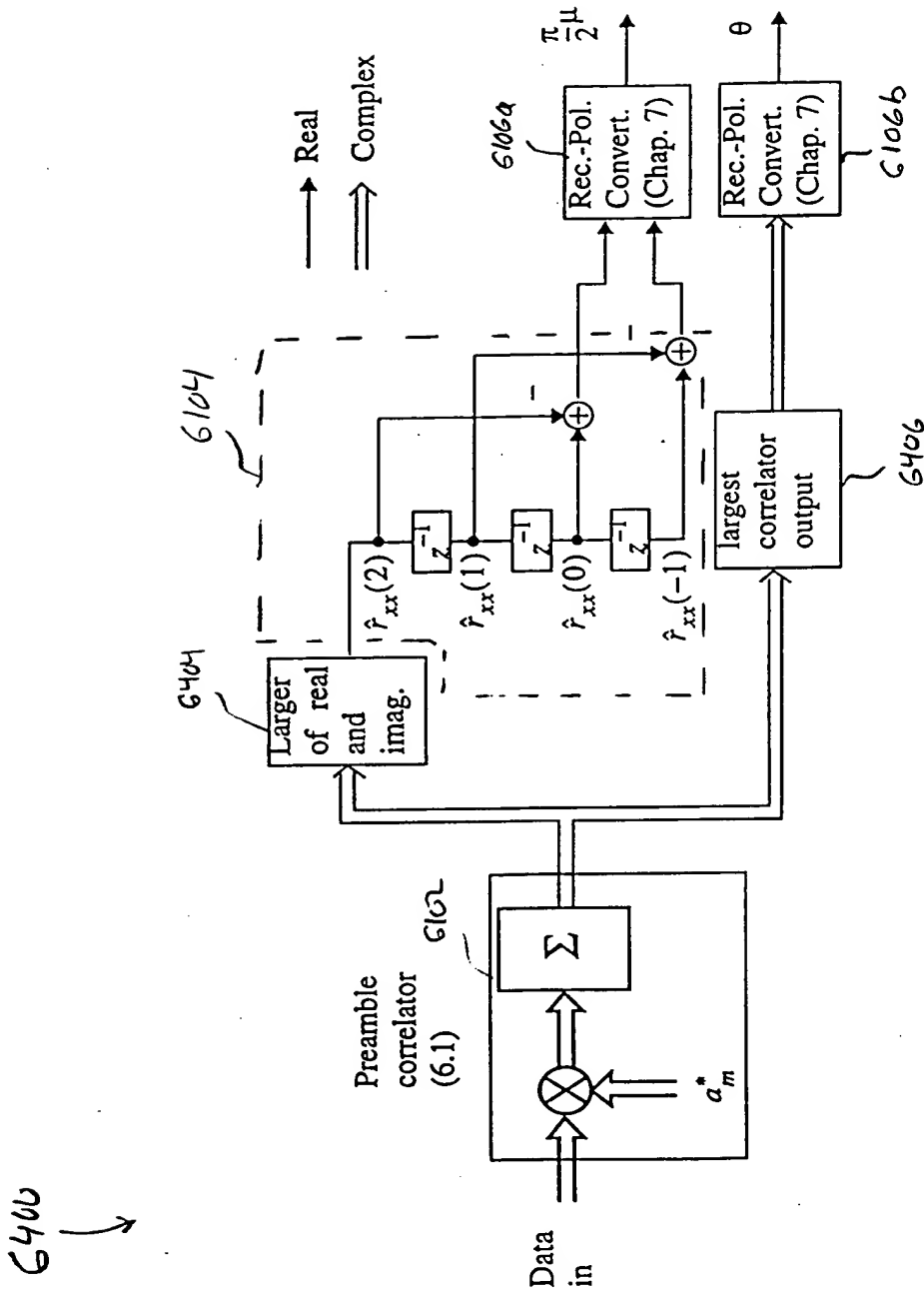


Fig. 64 Structure for carrier-phase and symbol timing recovery.

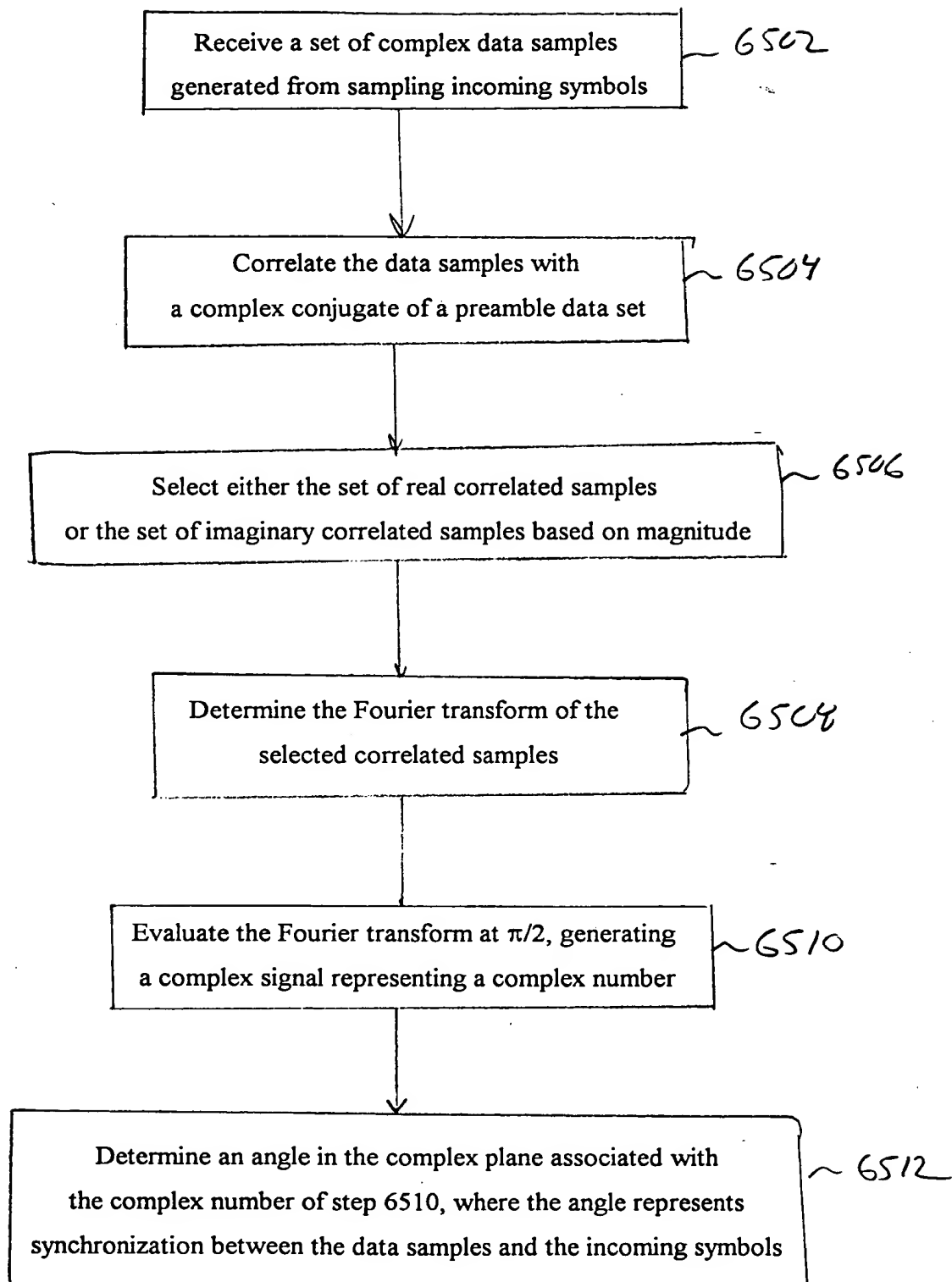


FIG. 65A

6500 (cont.)

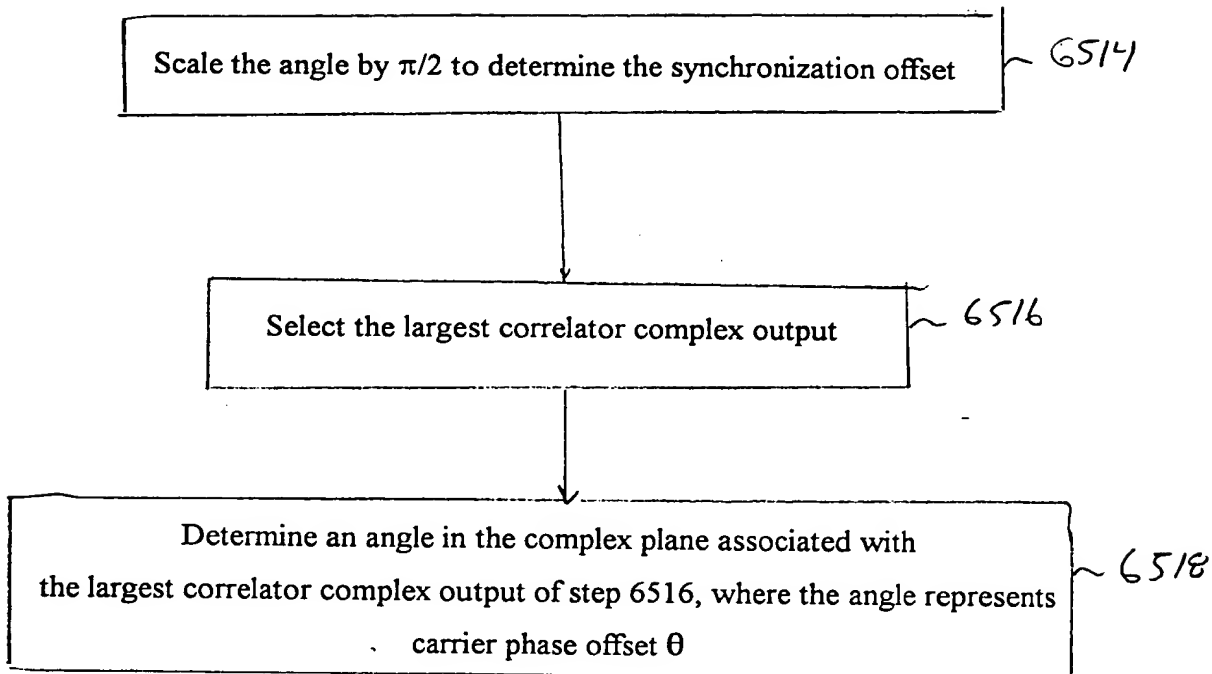


FIG. 65B

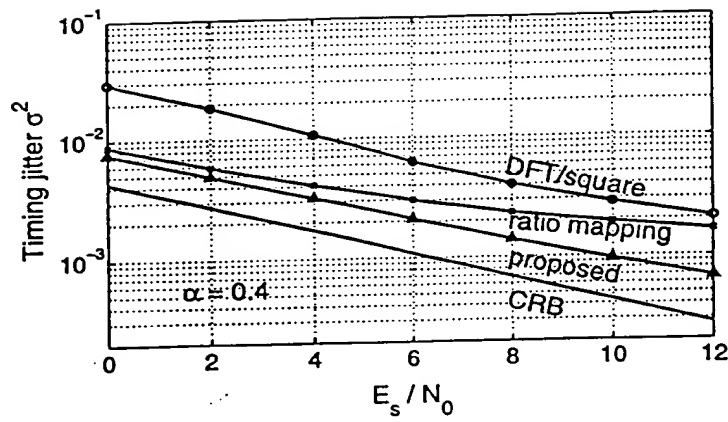


Figure 66: Timing jitter variance, $\alpha = 0.4$.

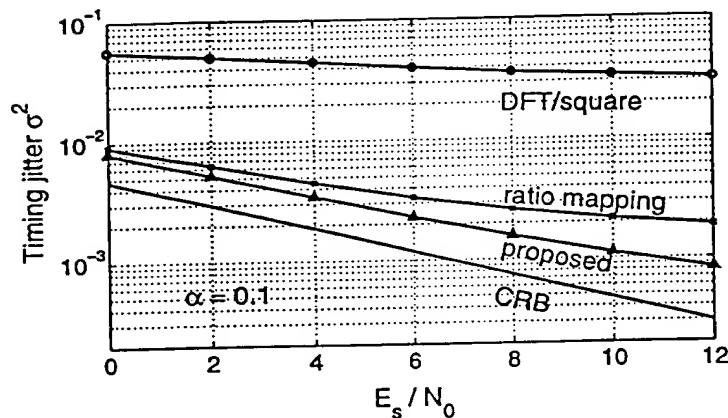


Figure 67: Timing jitter variance, $\alpha = 0.1$.

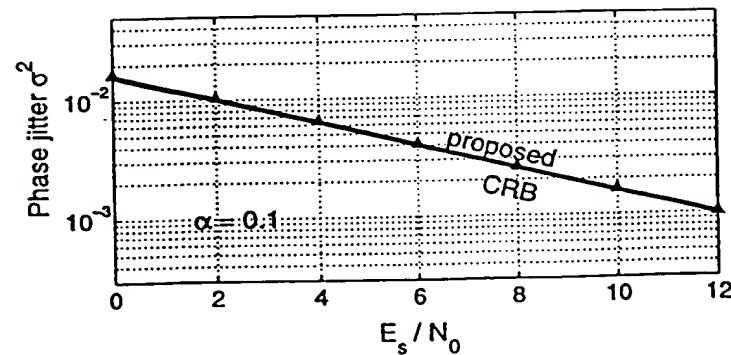


Figure 68: Phase jitter variance, $\alpha = 0.1$.

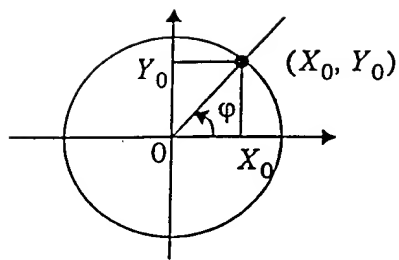


FIG. G1 Cartesian to polar conversion.

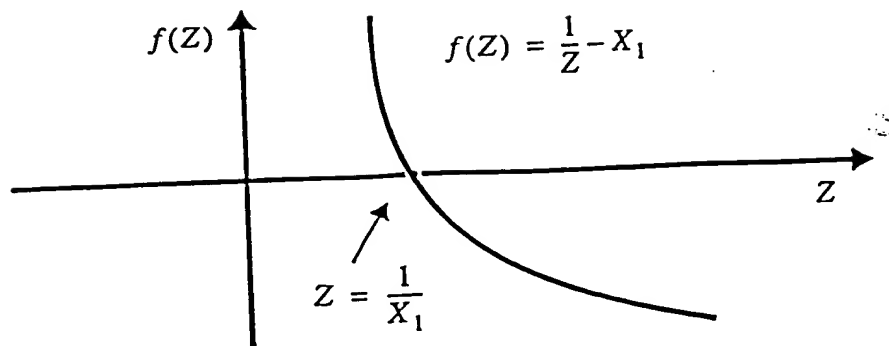


FIG. 70A: Using Newton-Raphson iteration to find $1/X_1$.

09698246 - 103000

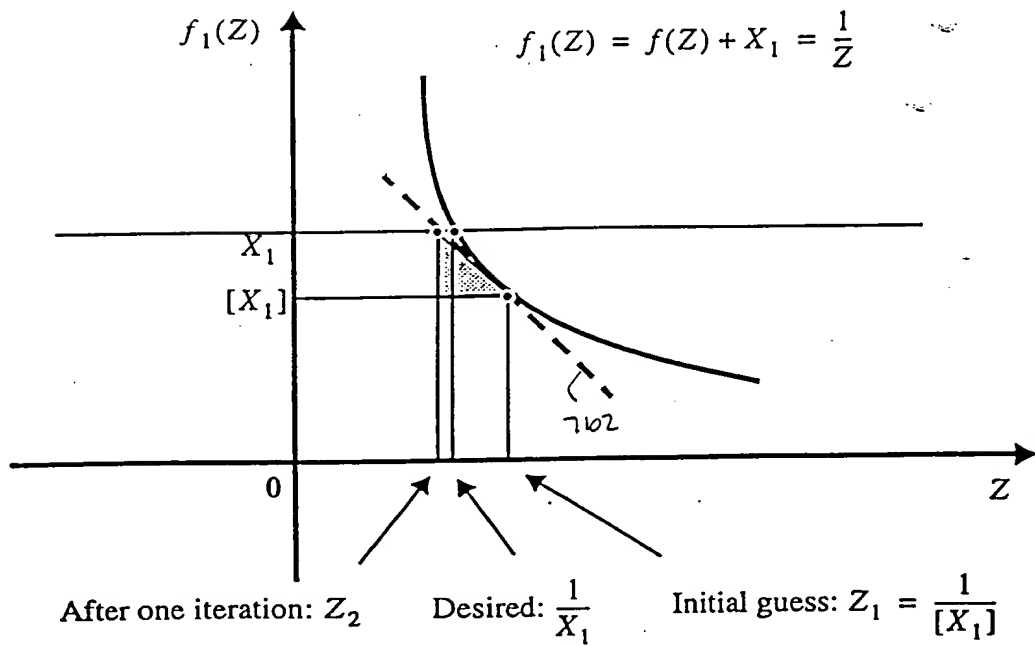


FIG. 70B: One Newton-Raphson iteration.

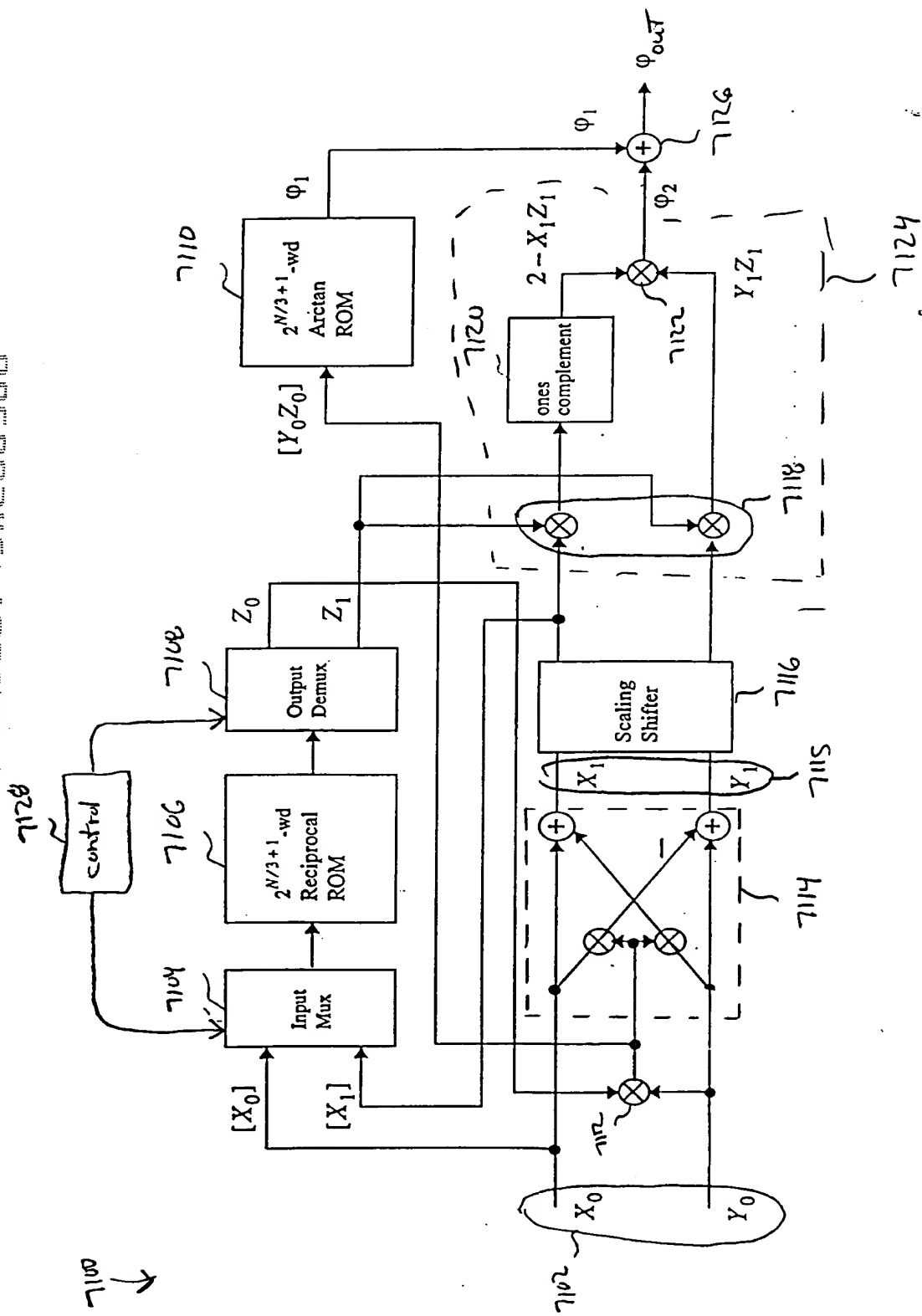


FIG. 71:

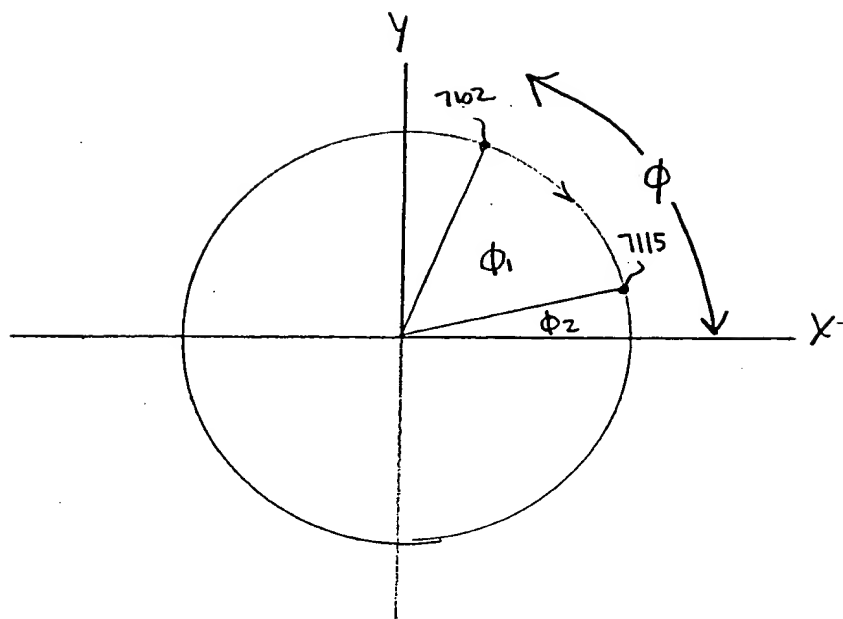


FIG. 72

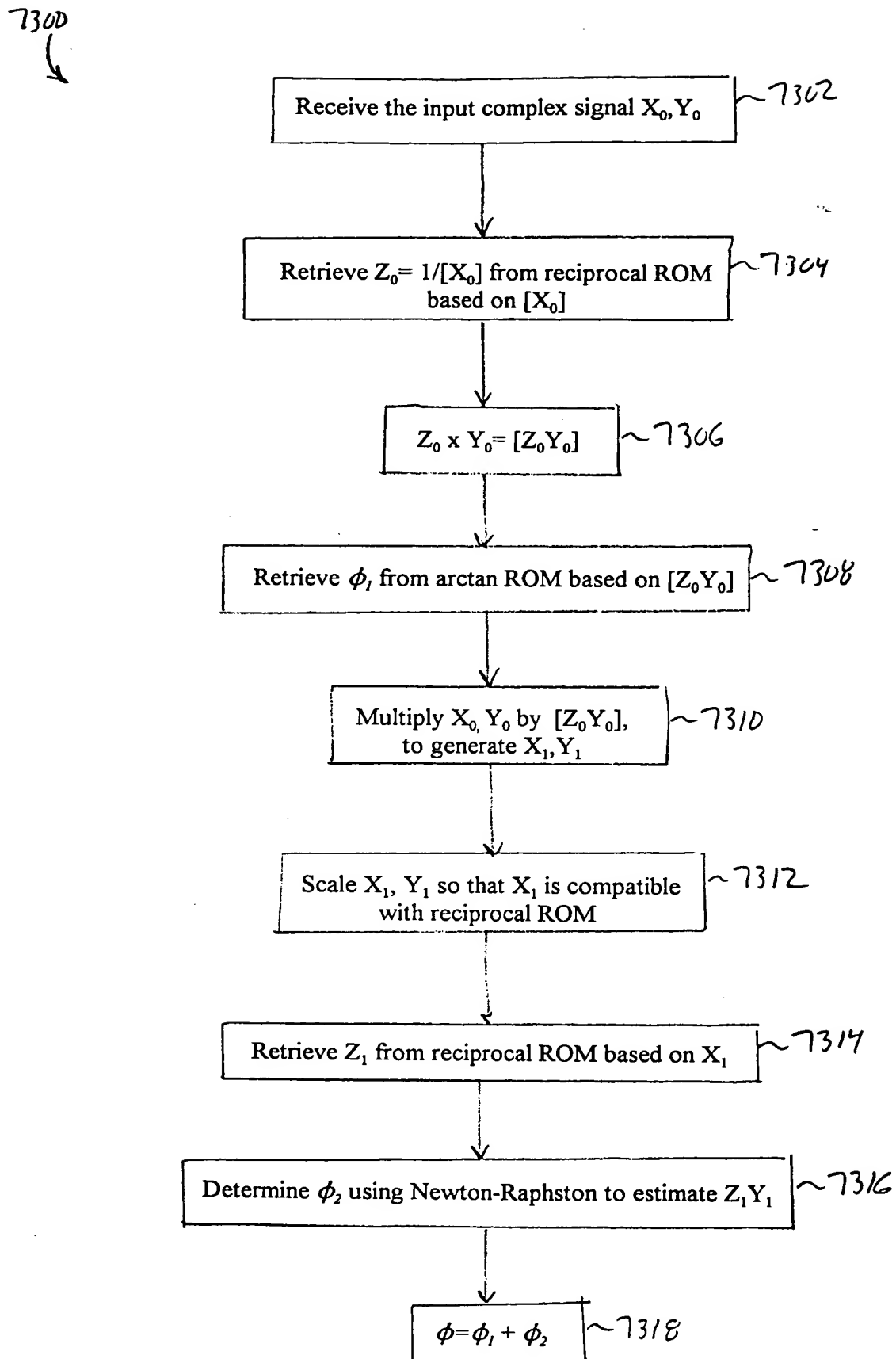


FIG. 73

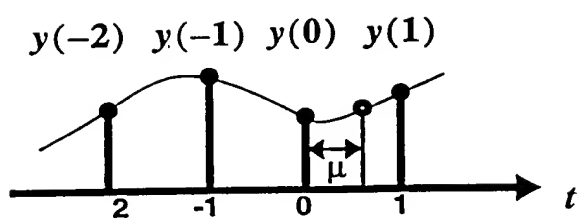


FIG. 74 Interpolation in a non-center interval.

0969844-103000

FIG 75A

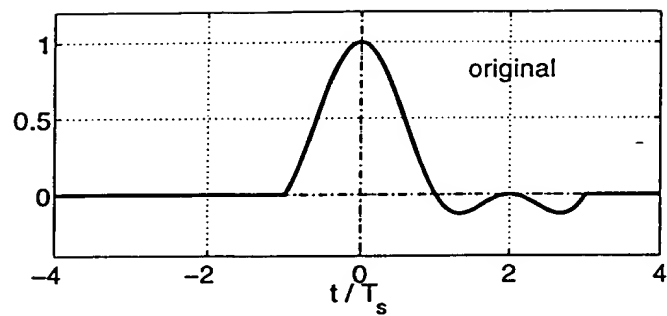


FIG 75B

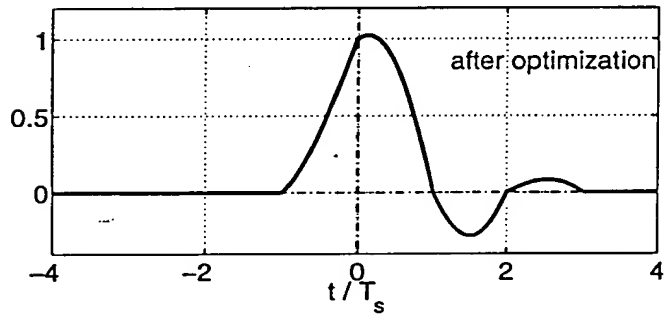


FIG 75A-B: Impulse responses of the non-center-interval interpolation filter A , before and B , after optimization.

FIG. 76A

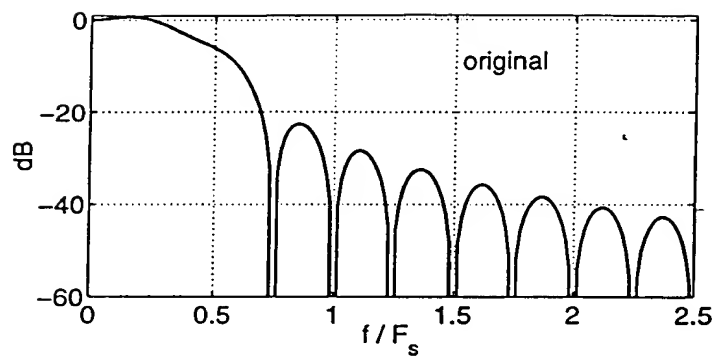


FIG. 76B

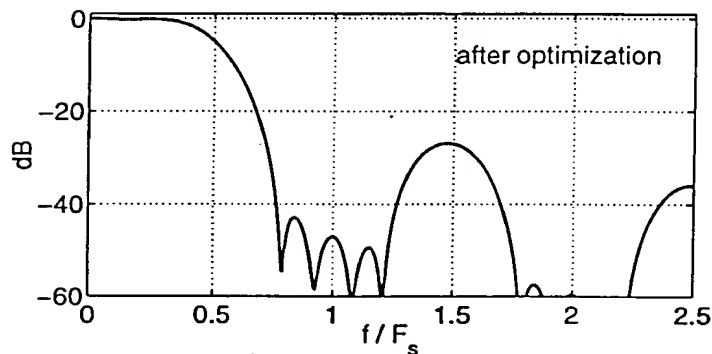


FIG. 76A - B : Frequency responses of the non-center-interval interpolator before optimization and , after optimization.

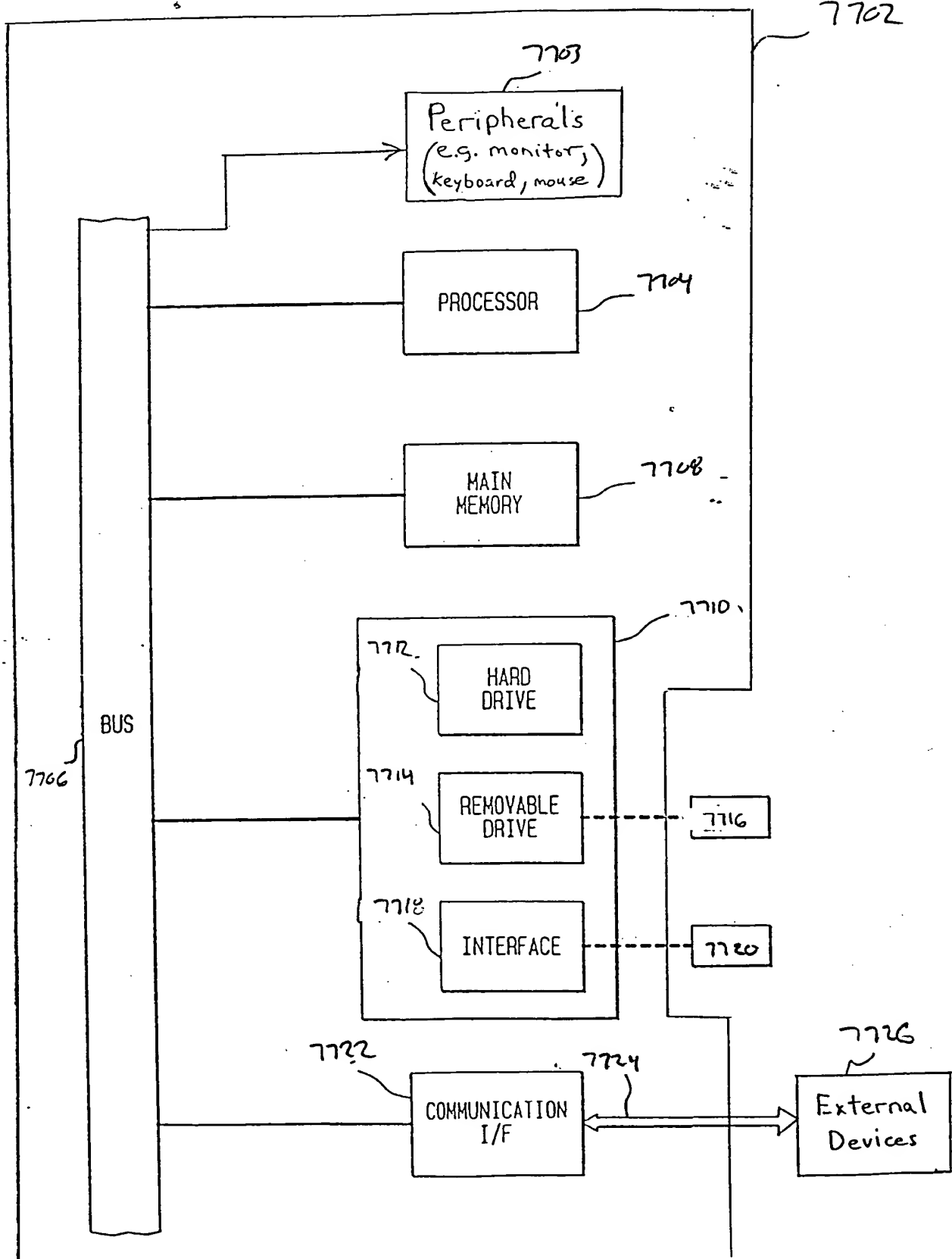


FIG. 77

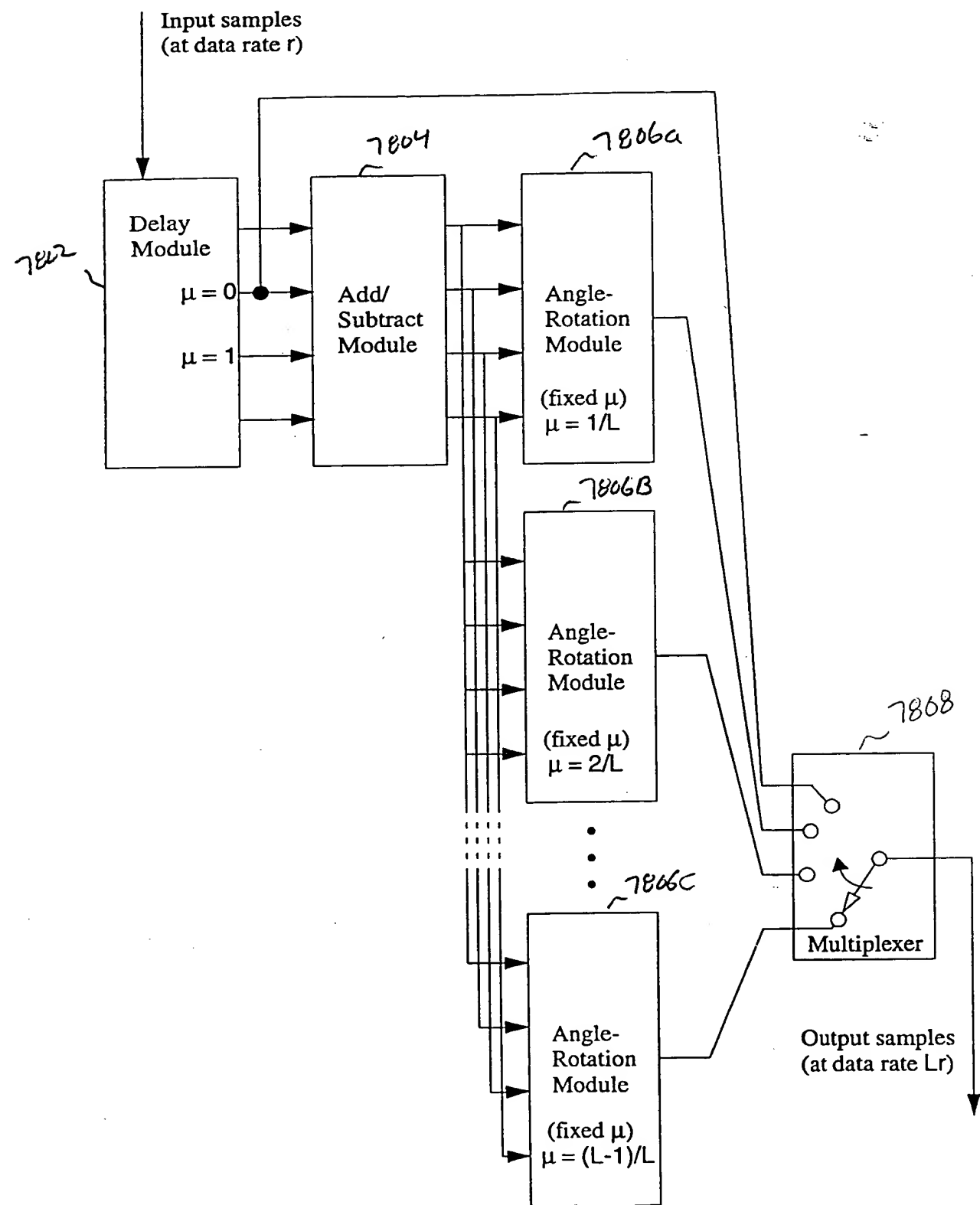


FIG. 78 Data Rate Expansion Circuit.

**This Page is Inserted by IFW Indexing and Scanning
Operations and is not part of the Official Record**

BEST AVAILABLE IMAGES

Defective images within this document are accurate representations of the original documents submitted by the applicant.

Defects in the images include but are not limited to the items checked:

- BLACK BORDERS**
- IMAGE CUT OFF AT TOP, BOTTOM OR SIDES**
- FADED TEXT OR DRAWING**
- BLURRED OR ILLEGIBLE TEXT OR DRAWING**
- SKEWED/SLANTED IMAGES**
- COLOR OR BLACK AND WHITE PHOTOGRAPHS**
- GRAY SCALE DOCUMENTS**
- LINES OR MARKS ON ORIGINAL DOCUMENT**
- REFERENCE(S) OR EXHIBIT(S) SUBMITTED ARE POOR QUALITY**
- OTHER:** _____

IMAGES ARE BEST AVAILABLE COPY.

As rescanning these documents will not correct the image problems checked, please do not report these problems to the IFW Image Problem Mailbox.